SUPPLEMENTARY INFORMATION

Noble metal-free catalytic decarboxylation of oleic acid to n-heptadecane on nickel-based metal-organic frameworks (MOFs)

L. Yang,[a†] B. W. McNichols,[b†] M. Davidson,[c] B. Schweitzer,[a] D.A. Gómez-Gualdrón,[a] B. G. Trewyn,[bc] A. Sellinger*[bc] and M. A. Carreon*[ac]

[a] Department of Chemical and Biological Engineering, Colorado School of Mines, Golden, CO 80401
[b] Department of Chemistry, Colorado School of Mines, Golden, CO 80401
[c] Materials Science Program, Colorado School of Mines, Golden, CO 80401
* Corresponding authors: aselli@mines.edu; mcarreon@mines.edu
† Authors are co-first author

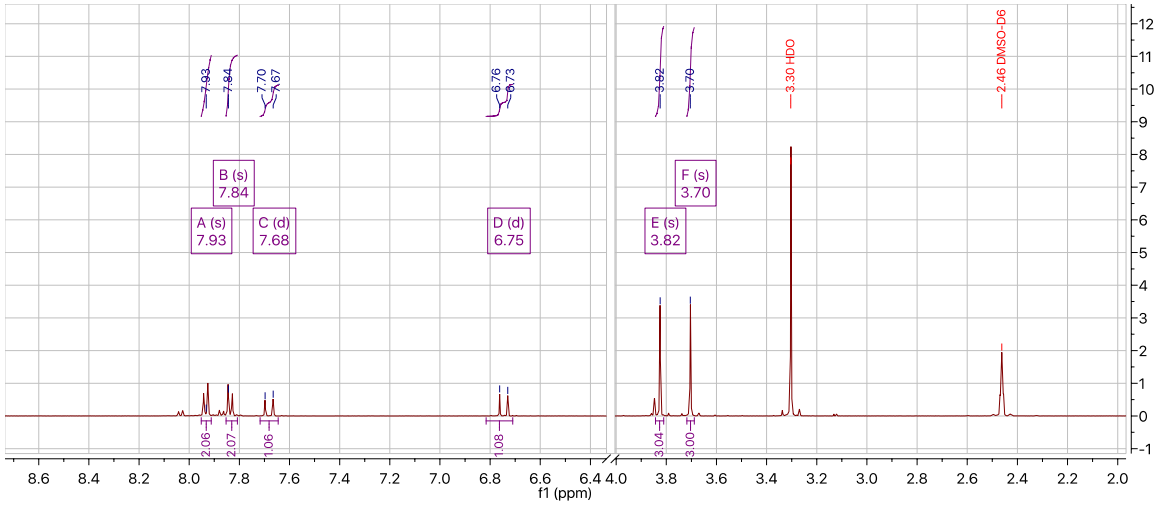

^{1}H NMR (500 MHz, DMSO-d_6) δ 7.93 (s, 2H), 7.84 (s, 2H), 7.68 (d, J = 16.0 Hz, 1H), 6.75 (d, J = 16.0 Hz, 1H), 3.82 (s, 3H), 3.70 (s, 3H).

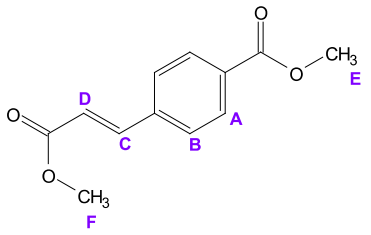

Figure S1. BM65 precursor - methyl (*E*)-4-(3-methoxy-3-oxoprop-1-en-1-yl)benzoate ^{1}H NMR (500 MHz, DMSO-d6)

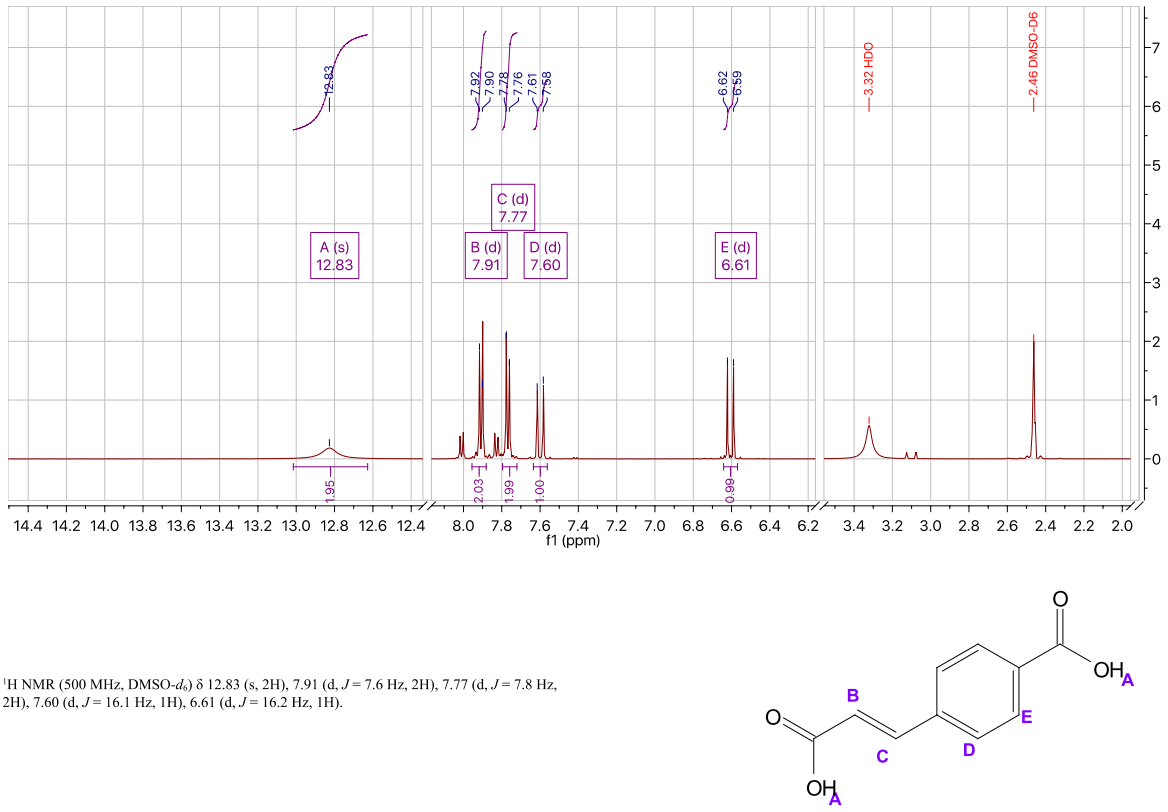

^{1}H NMR (500 MHz, DMSO-d_6) δ 12.83 (s, 2H), 7.91 (d, J = 7.6 Hz, 2H), 7.77 (d, J = 7.8 Hz, 2H), 7.60 (d, J = 16.1 Hz, 1H), 6.61 (d, J = 16.2 Hz, 1H).

Figure S2. BM65 - (*E*)-4-(2-carboxyvinyl)benzoic acid ^{1}H NMR (500 MHz, DMSO-d_6)

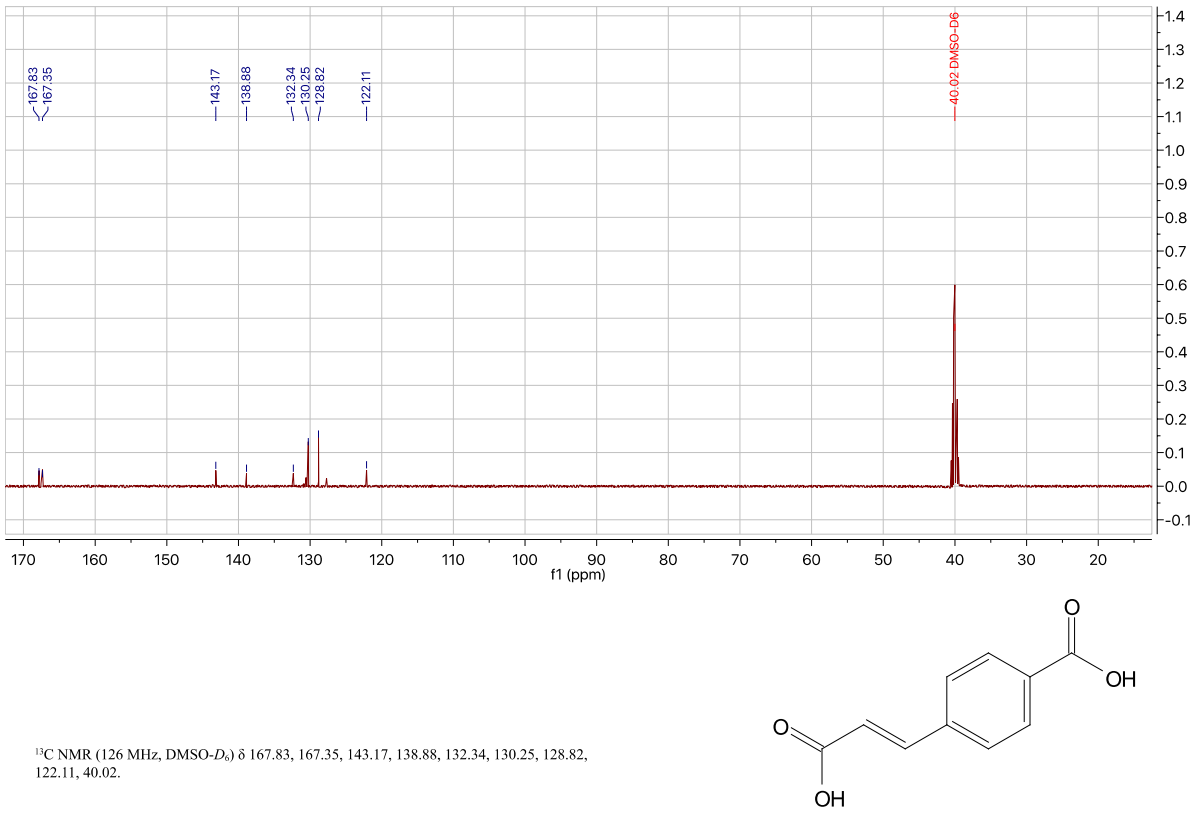

^{13}C NMR (126 MHz, DMSO-D_6) δ 167.83, 167.35, 143.17, 138.88, 132.34, 130.25, 128.82, 122.11, 40.02.

Figure S3. BM65 - (*E*)-4-(2-carboxyvinyl)benzoic acid ^{13}C NMR (126 MHz, DMSO-D_6)

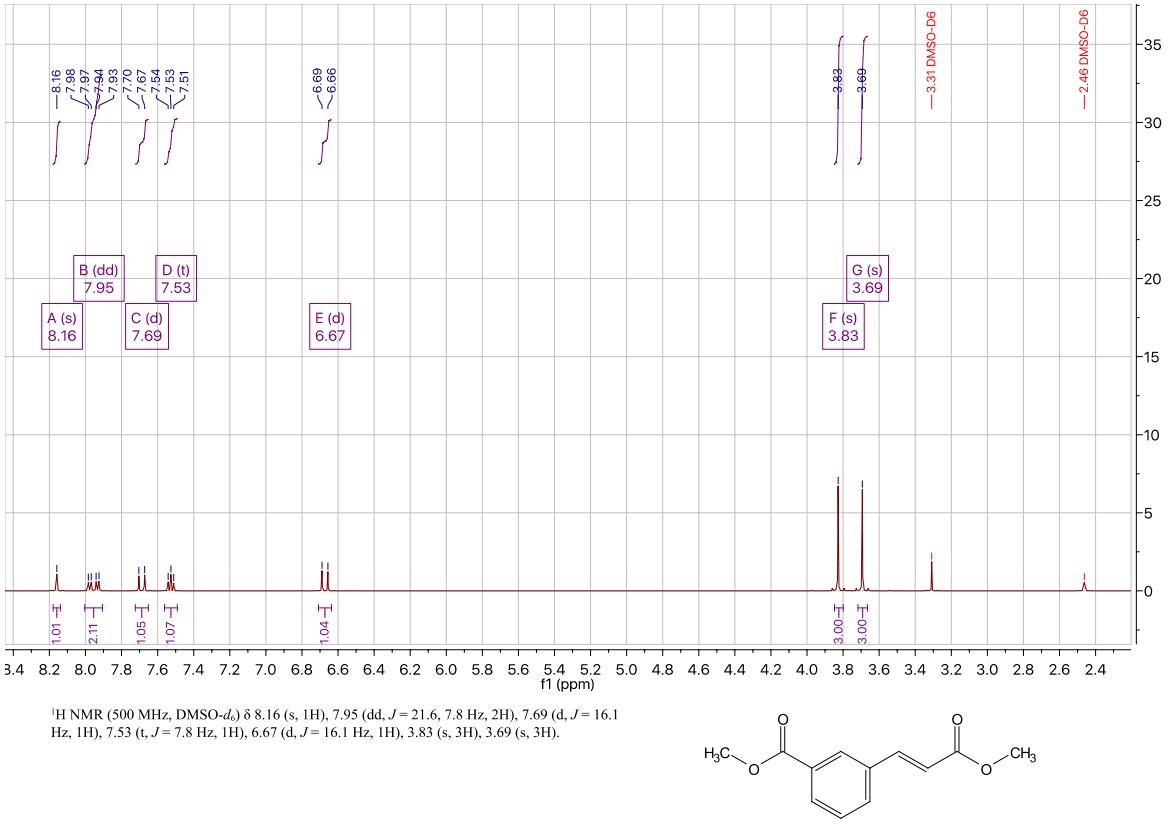

^{1}H NMR (500 MHz, DMSO-d_6) δ 8.16 (s, 1H), 7.95 (dd, J = 21.6, 7.8 Hz, 2H), 7.69 (d, J = 16.1 Hz, 1H), 7.53 (t, J = 7.8 Hz, 1H), 6.67 (d, J = 16.1 Hz, 1H), 3.83 (s, 3H), 3.69 (s, 3H).

Figure S4. BM73 – precursor - methyl (*E*)-3-(3-methoxy-3-oxoprop-1-en-1-yl)benzoate (500 MHz, DMSO-d6)

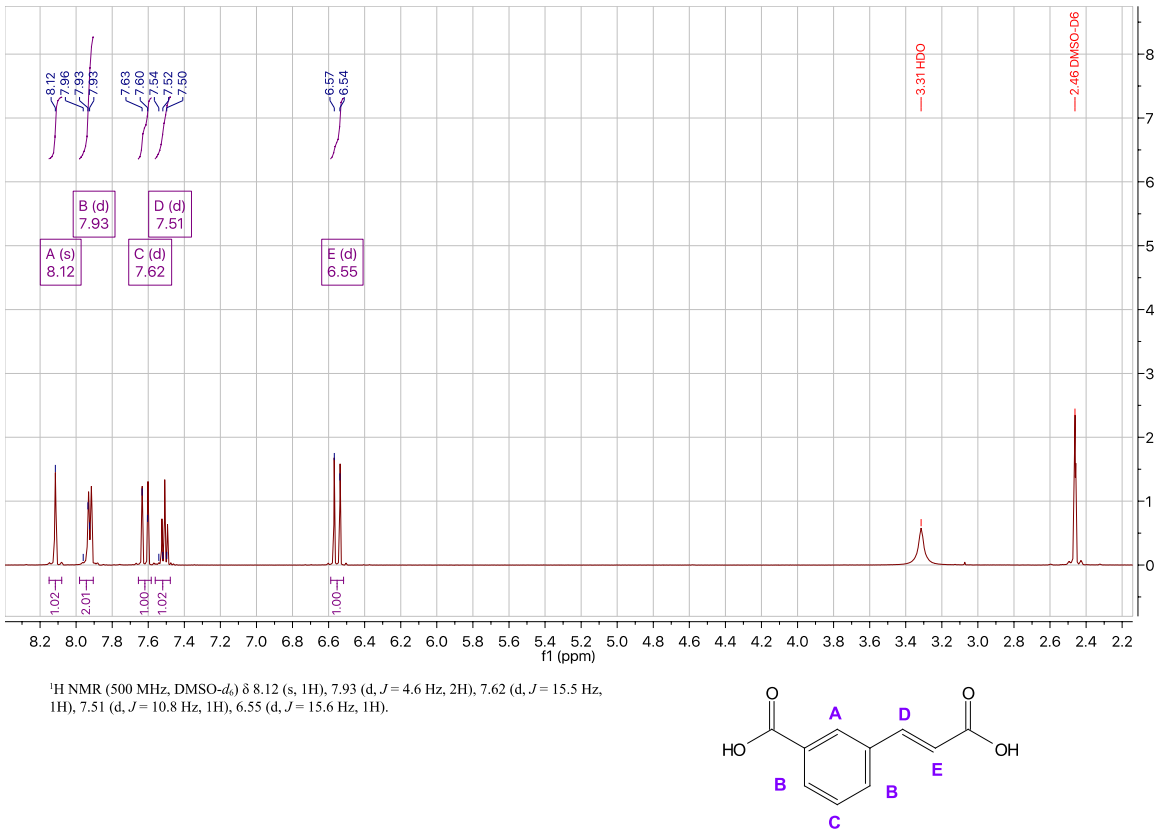

^{1}H NMR (500 MHz, DMSO-d_6) δ 8.12 (s, 1H), 7.93 (d, J = 4.6 Hz, 2H), 7.62 (d, J = 15.5 Hz, 1H), 7.51 (d, J = 10.8 Hz, 1H), 6.55 (d, J = 15.6 Hz, 1H).

Figure S5. BM73 - (*E*)-3-(2-carboxyvinyl)benzoic acid ^{1}H NMR (500 MHz, DMSO-d_6)

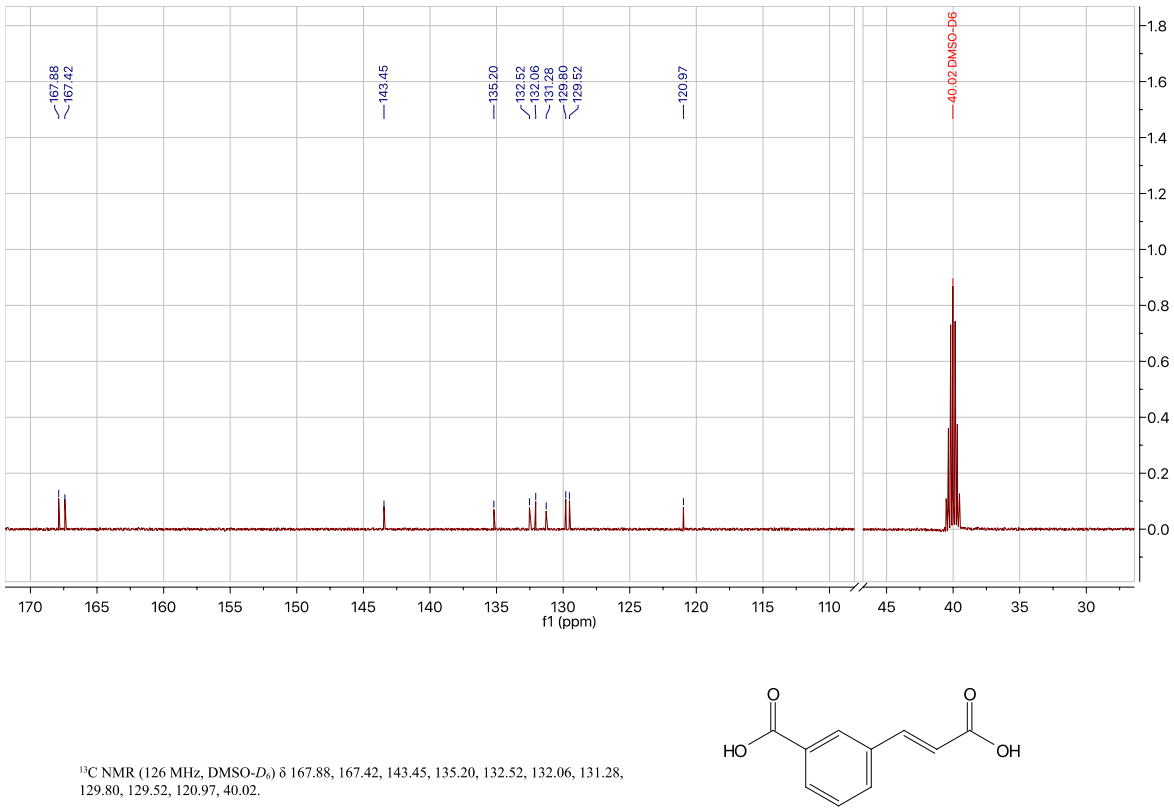

^{13}C NMR (126 MHz, DMSO-D_6) δ 167.88, 167.42, 143.45, 135.20, 132.52, 132.06, 131.28, 129.80, 129.52, 120.97, 40.02.

Figure S6. BM73 - (*E*)-3-(2-carboxyvinyl)benzoic acid ^{13}C NMR (126 MHz, DMSO-D_6)

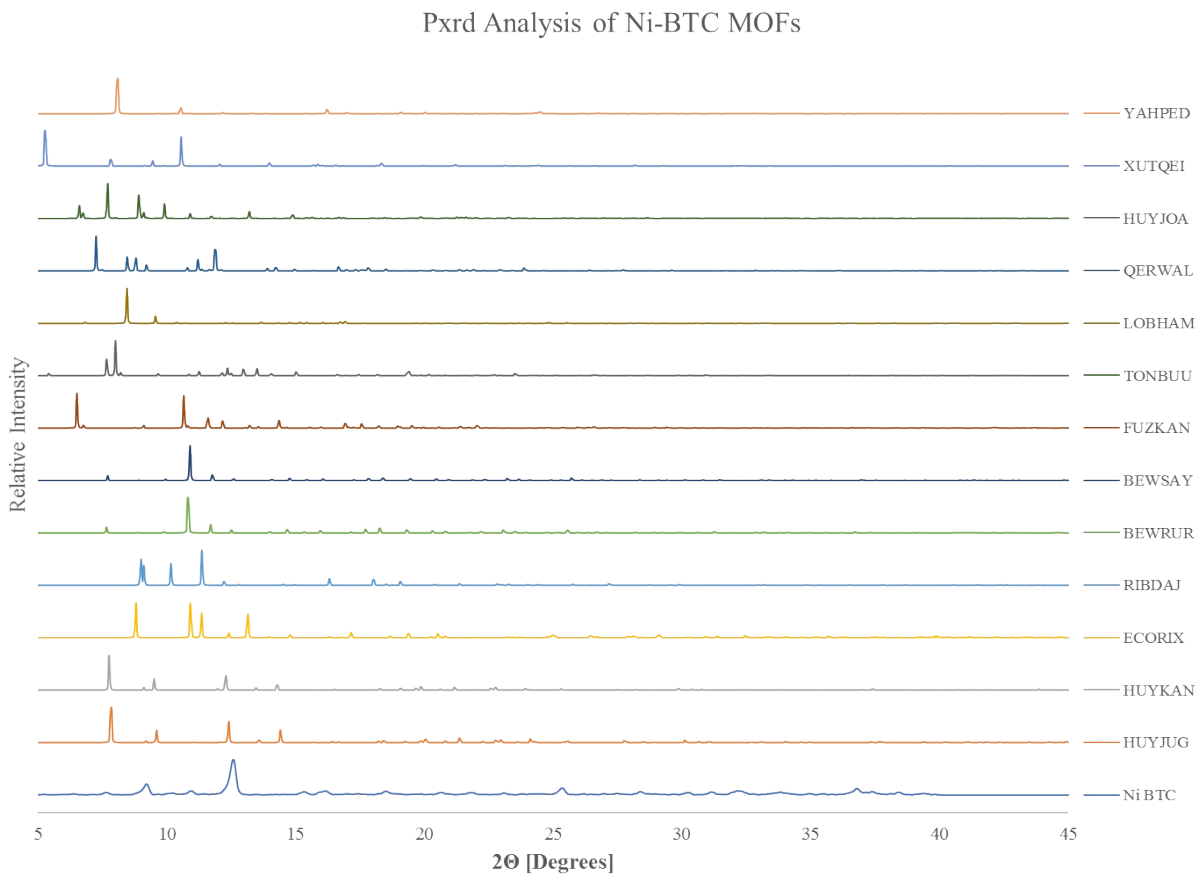

Figure S7. Comparison of experimentally collected PXRD pattern for our Ni-BTC with simulated patterns in all Ni-BTC variants encountered in the CoRE MOF database. In this plot, the experimental PXRD pattern underwent background stripping, Gaussian smoothing, and relative scaling using the Reflex Powder Processing Module in Materials Studio [1]. Simulated PXRD patterns for nickel MOFs from the CoRE MOF database [2] were obtained with the Reflex Materials Studio Module.

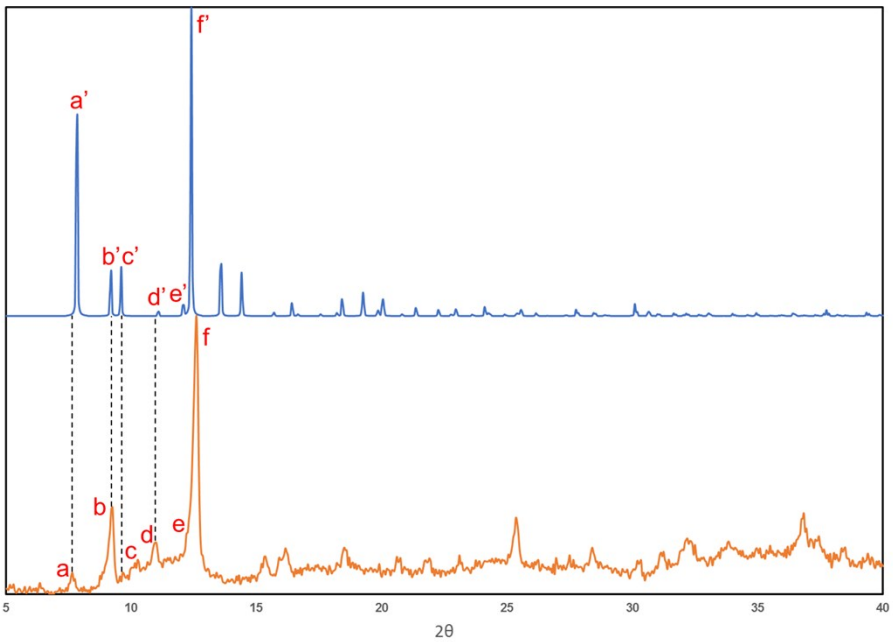

Figure S8. Comparison between "as-is" experimental pattern for Ni-BTC (blue) and simulated pattern for HUYJUG (orange). Coordinating solvent originally found in the reported HUYJUG structure was replaced by ethanol and water based on the solvent used for Ni-BTC synthesis in this work.

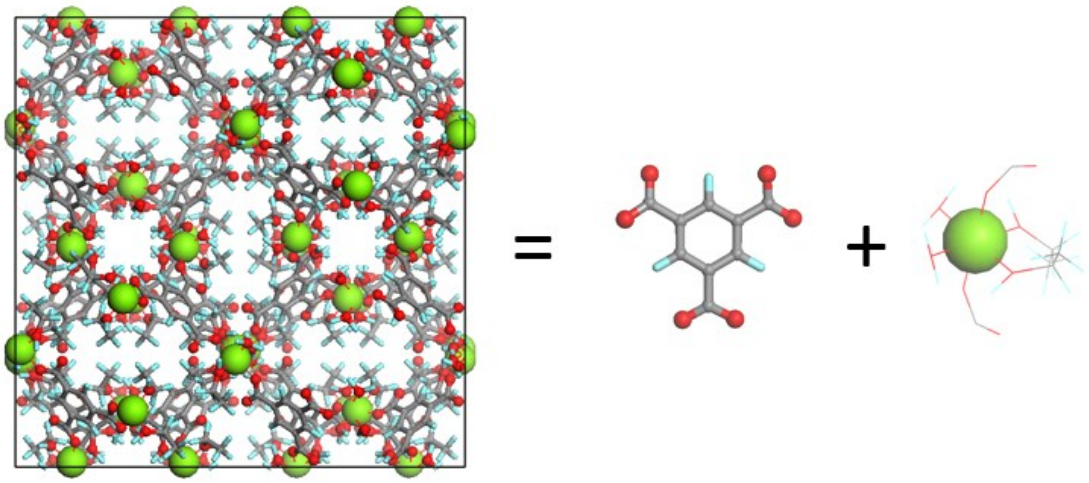

Figure S9. Snapshot of HUYJUG structure and its constituent building blocks: trimesic acid and six-coordinated, octahedral nickel ion. Each nickel ion is coordinated to four neutral solvents and two carboxylate groups, giving nickel a 2+ oxidation state. nickel: green, oxygen: red, carbon: gray, hydrogen: light blue. The nickel to linker ratio in HUYJUG is 1 and the experimental nickel to linker ratio in Ni-BTC is 1.4.

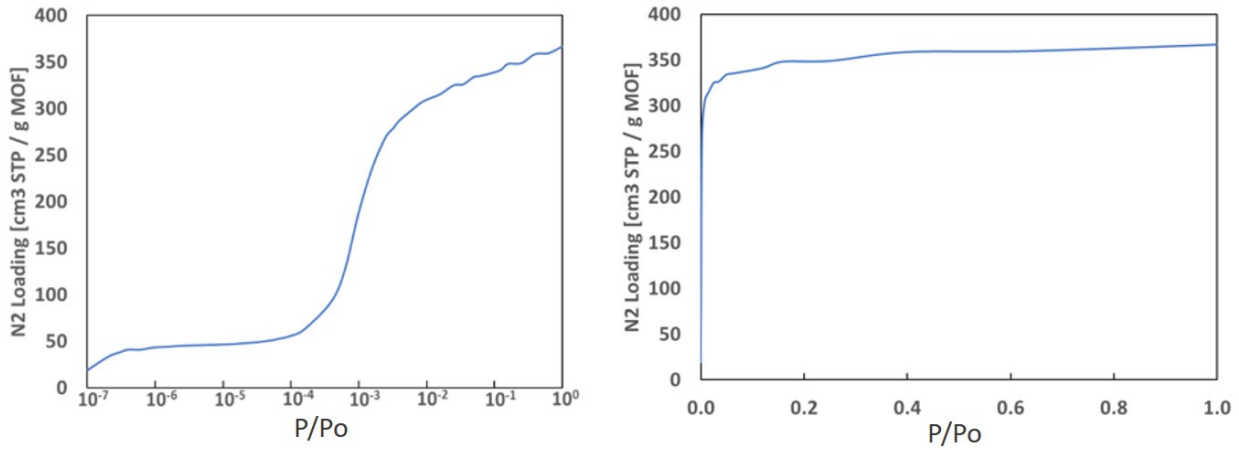

Figure S10.Simulated nitrogen isotherm on HUYJUG structure. Left: isotherm in semi-log scale. Right: isotherm in absolute scale. Isotherms were obtained through grand canonical Monte Carlo (GCMC) simulations using the RASPA code[3]. Intermolecular interactions were described by assigning Universal Force Field [4] parameters for MOF atoms and TraPPE force field [5] parameters for nitrogen molecules.

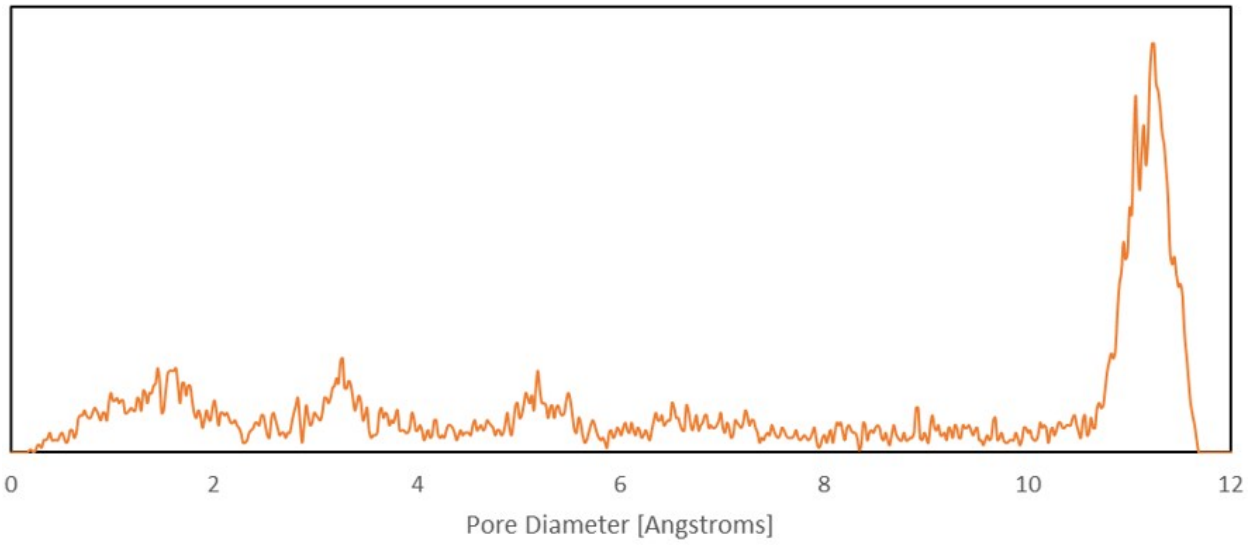

Figure S11. Geometrically-calculated pore size distribution of HUYJUG. Calculation follows the method outlined by Gelb and Gubbins [6].

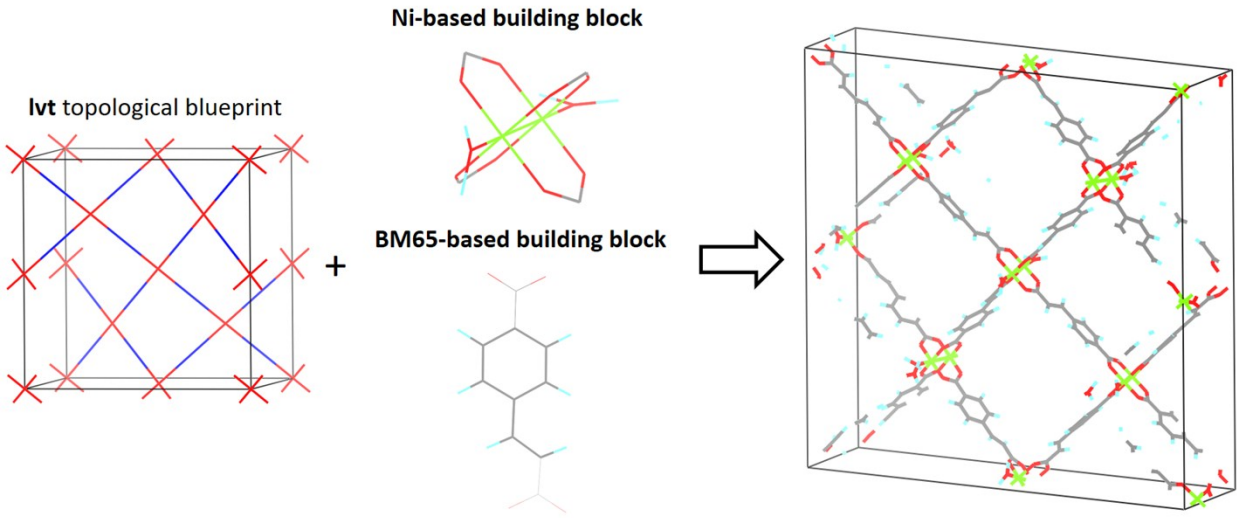

Figure S12. Automated computational construction of a MOF based on the BM65 linker, Ni paddlewheel and **lvt** topological blueprint. Construction was done using the topologically-based crystal constructor (ToBaCCo) code [7].

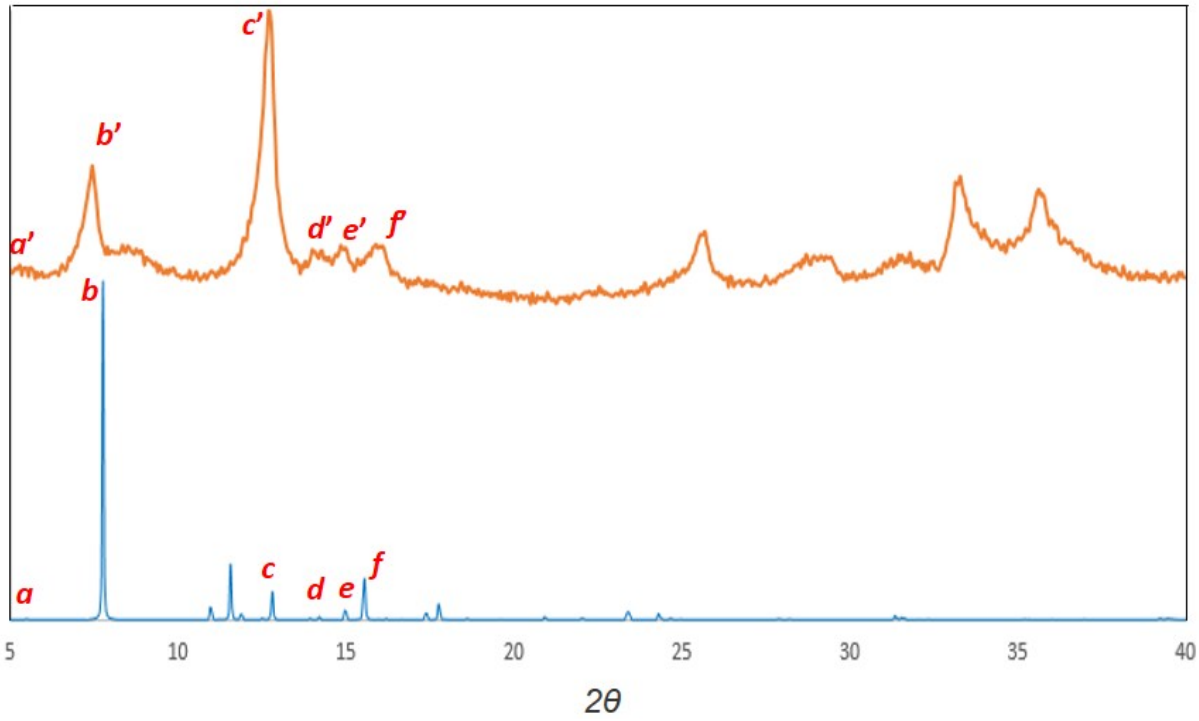

Figure S13. Comparison between "as-synthesized" experimental pattern for Ni-BM65 (blue) and simulated pattern for **lvt**-Ni-BM65 created by the ToBaCCo code (orange).

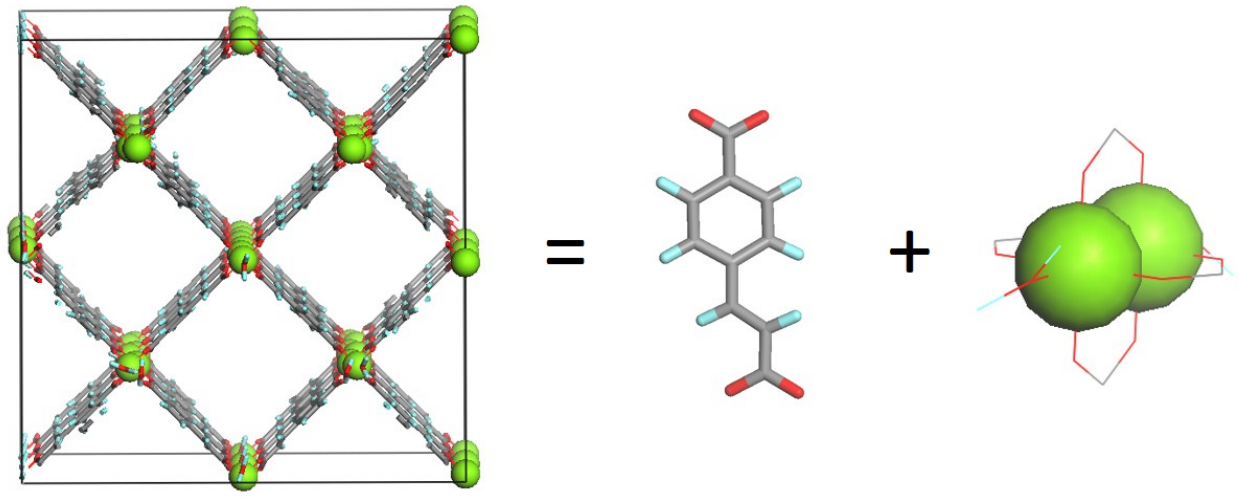

Figure S14. Snapshot of **lvt**-Ni-BM65 structure and its constituent building blocks: trimesic acid and six-coordinated, nickel paddlewheel. The two nickel ion are coordinated to two neutral solvents and four carboxylate groups, giving the nickel ions a 2+ oxidation state. nickel: green, oxygen: red, carbon: gray, hydrogen: light blue. The linker to node ratio in **lvt**-Ni-BM65 is 1 and the experimental linker to node ratio in Ni-BM65 is 1.1.

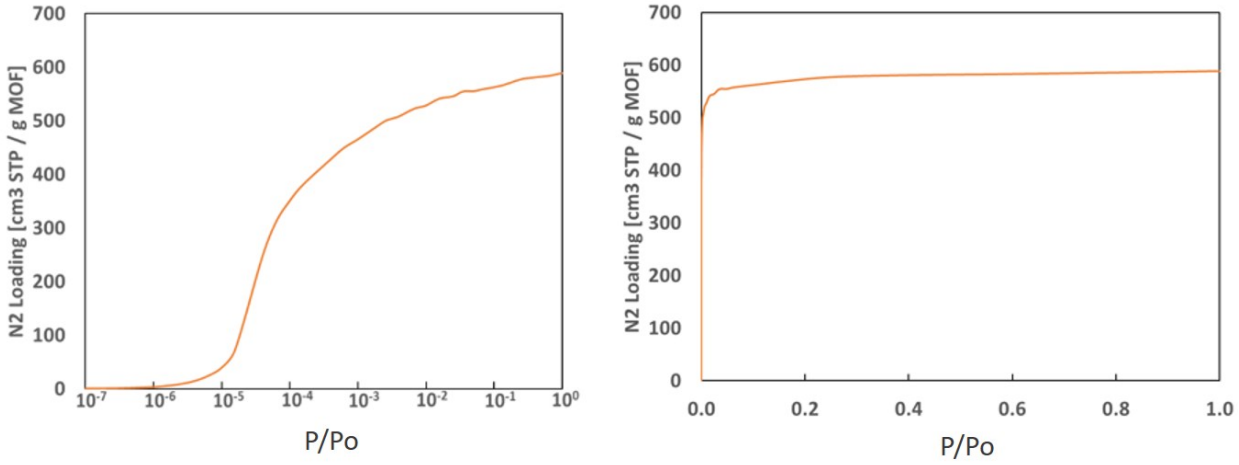

Figure S15. Simulated nitrogen isotherm on **lvt**-Ni-BM65 structure. Left: isotherm in semi-log scale. Right: isotherm in absolute scale. Isotherms were obtained through grand canonical Monte Carlo (GCMC) simulations using the RASPA code [3]. Intermolecular interactions were described by assigning Universal Force Field [4] parameters for MOF atoms and TraPPE force field [5] parameters for nitrogen molecules.

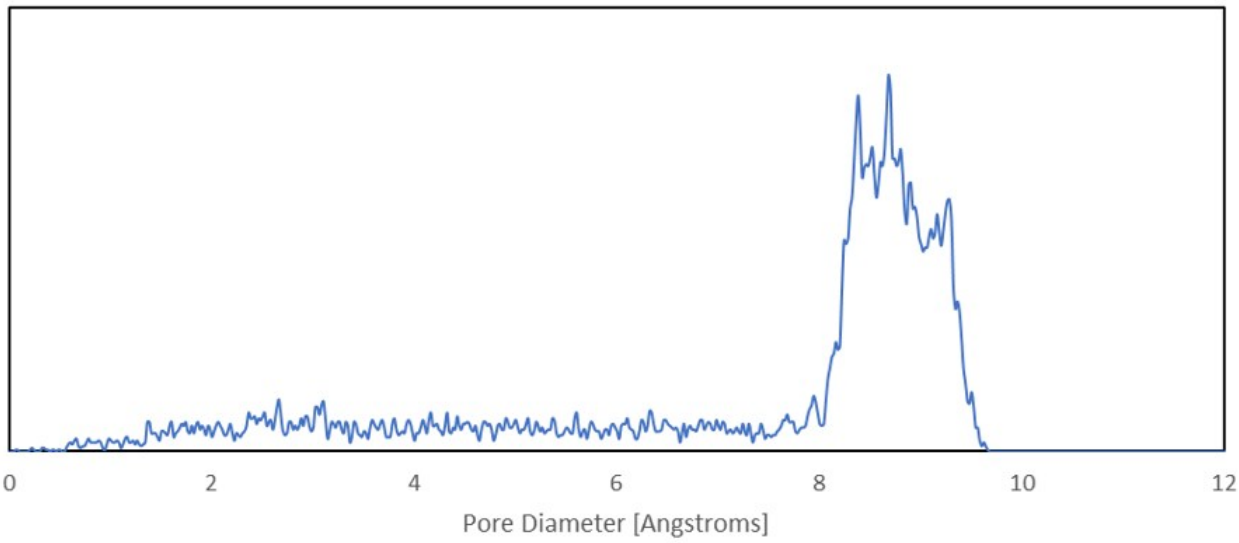

Figure S16. Geometrically-calculated pore size distribution of **lvt**-NI-BM65. Calculation follows the method outlined by Gelb and Gubbins [6].

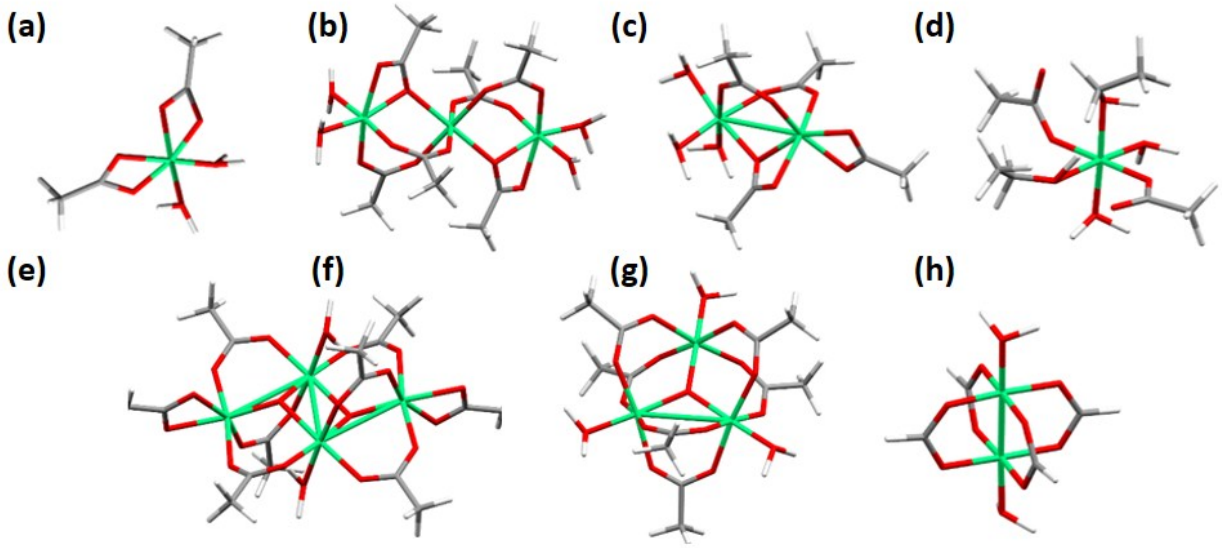

Figure S17. Examples of nickel nodes encountered in synthesized MOFs from the CoRE MOF database. HUYJUG is based on node (d) and **lvt**-Ni-BM65 is based on node (h). DFT calculations on the latter two nodes show each node to present two unpaired electrons. DFT calculations show an electronic charge of +0.95 at the nickel atom in the node of HUYJUG and +0.56 and +0.73 in the nickel atoms in the node of **lvt**-Ni-BM65. DFT calculations were performed with the Gaussian 09 program [9] using the M06 functional [9] with the Def2TZVP basis set for nickel and the 6-31g basis set for CHO atoms. Charges were obtained according to natural bond order analysis (nbo).

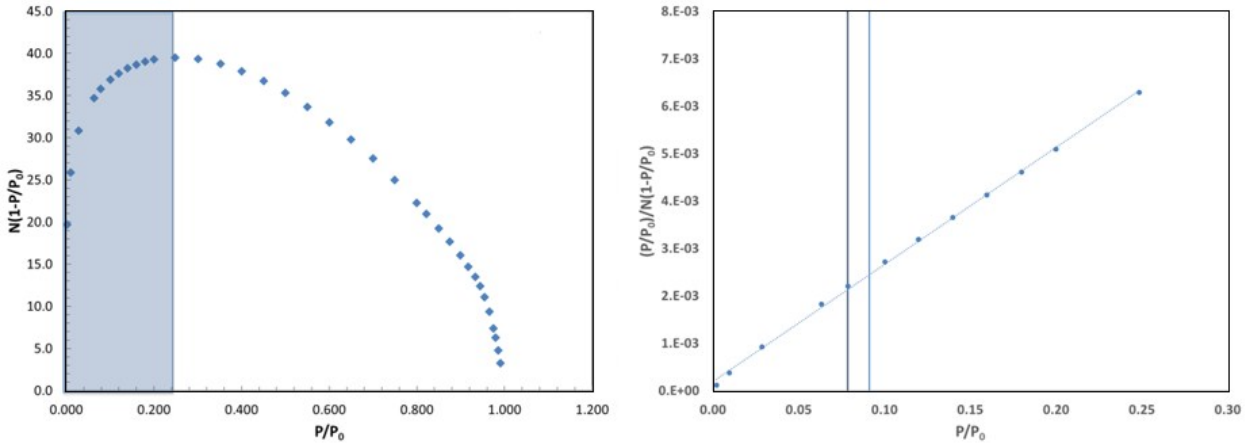

Figure S18. BET area calculation from measured nitrogen isotherm in Ni-BM 65. Left: Plot illustrating the pressure range selection for the BET area calculation to fulfill first and second BET consistency criterion. Right: BET area calculation in selected pressure range. Vertical lines indicate the pressure P_m corresponding to monolayer loading estimated from BET theory (to fulfill the third BET consistency criterion, it should fall within pressure range used for the linear regression) and the pressure equal to $1/(C^{1/2} + 1)$ (to fulfill the fourth BET consistency criterion both vertical lines should be within 20% of each other). N_m = 40 cm^3(STP)/g, C = 137.7, P_m = 0.079. BET area = 175 m^2/g.

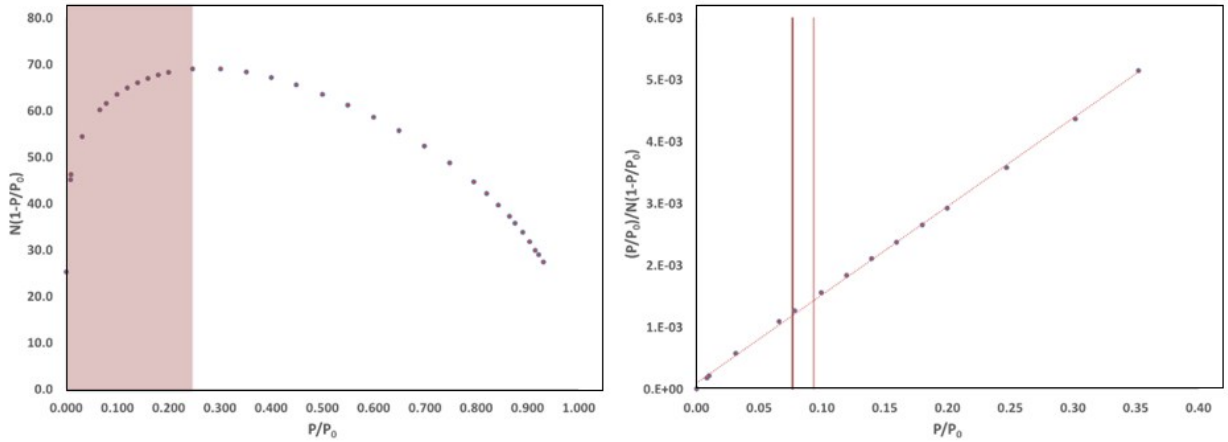

Figure S19. BET area calculation from measured nitrogen isotherm in Ni-BM 73. Left: Plot illustrating the pressure range selection for the BET area calculation to fulfill first and second BET consistency criterion. Right: BET area calculation in selected pressure range. Vertical lines indicate the pressure P_m corresponding to monolayer loading estimated from BET theory (to fulfill the third BET consistency criterion, it should fall within pressure range used for the linear regression) and the pressure equal to $1/(C^{1/2} + 1)$ (to fulfill the fourth BET consistency criterion both vertical lines should be within 20% of each other). N_m = 70 cm^3(STP)/g, C = 145.4, P_m = 0.077. BET area = 301 m^2/g.

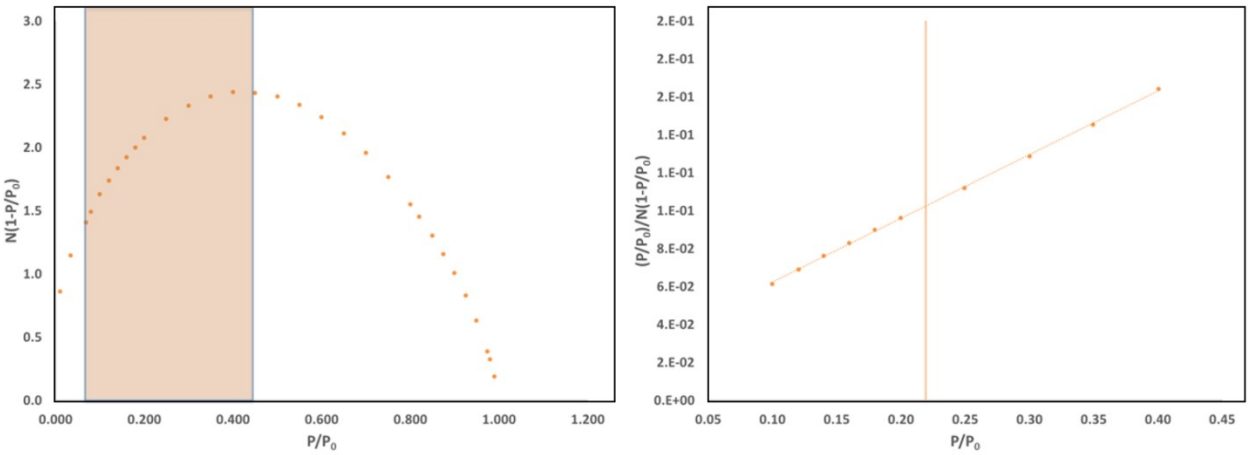

Figure S20. BET area calculation from measured nitrogen isotherm in Ni-BTC. Left: Plot illustrating the pressure range selection for the BET area calculation to fulfill first and second BET consistency criterion. Right: BET area calculation in selected pressure range. Vertical lines indicate the pressure P_m corresponding to monolayer loading estimated from BET theory (to fulfill the third BET consistency criterion, it should fall within pressure range used for the linear regression) and the pressure equal to $1/(C^{1/2} + 1)$ (to fulfill the fourth BET consistency criterion both vertical lines should be within 20% of each other). N_m = 3 cm^3(STP)/g, C = 12.7, P_m/P_0 = $1.50 * 10^{-3}$. BET area = 12 m^2/g.

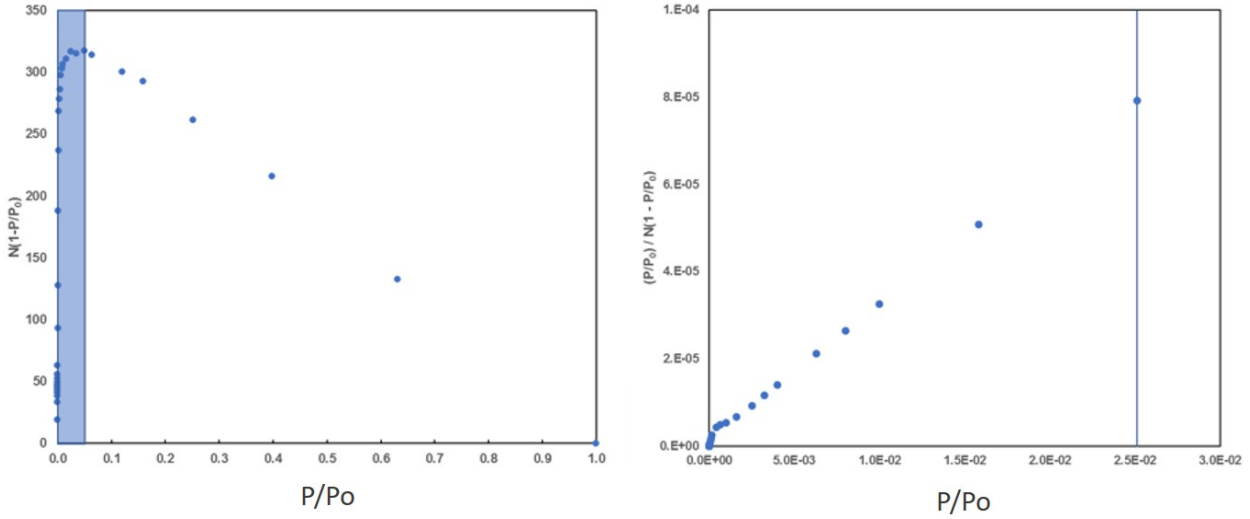

Figure S21. BET area calculation from simulated nitrogen isotherm in HUYJUG. Left: Plot illustrating the pressure range selection for the BET area calculation to fulfill first and second BET consistency criterion. Right: BET area calculation in selected pressure range. Vertical lines indicate the pressure P_m corresponding to monolayer loading estimated from BET theory (to fulfill the third BET consistency criterion, it should fall within pressure range used for the linear regression) and the pressure equal to $1/(C^{1/2} + 1)$ (to fulfill the fourth BET consistency criterion both vertical lines should be within 20% of each other). N_m = 317.2 cm^3(STP)/g, C = 3569.6, P_m/P_0 = 0.01646. BET area = 1381.4 m^2/g.

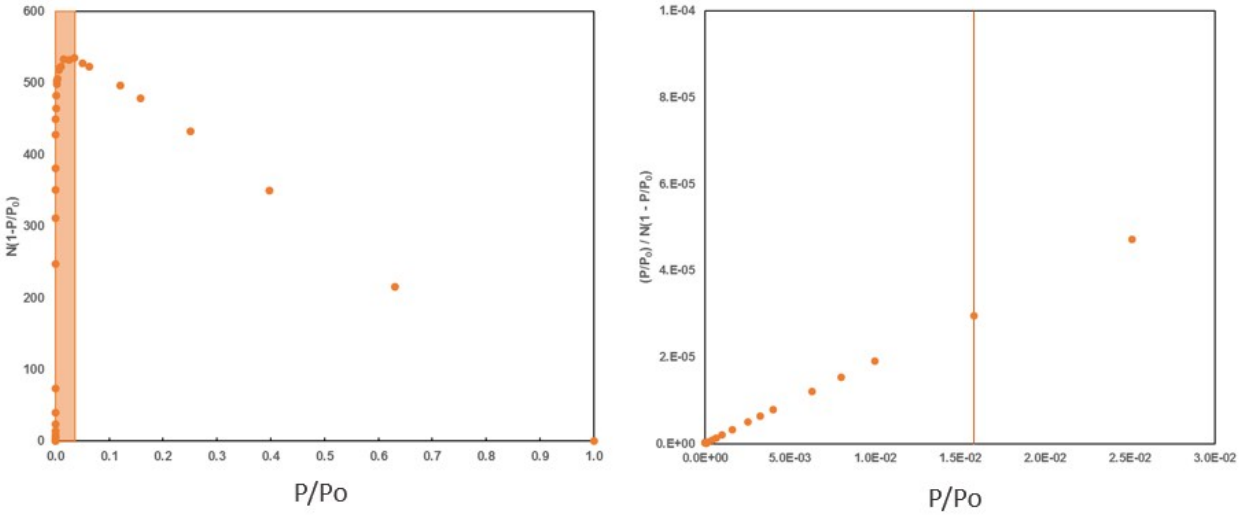

Figure S22. BET area calculation from simulated nitrogen isotherm in **lvt**-Ni-BM65. Left: Plot illustrating the pressure range selection for the BET area calculation to fulfill first and second BET consistency criterion. Right: BET area calculation in selected pressure range. Vertical lines indicate the pressure P_m corresponding to monolayer loading estimated from BET theory (to fulfill the third BET consistency criterion, it should fall within pressure range used for the linear regression) and the pressure equal to $1/(C^{1/2} + 1)$ (to fulfill the fourth BET consistency criterion both vertical lines should be within 20% of each other). N_m = 533.2 cm^3(STP)/g, C = 7430.8, P_m/P_0 = 0.01147. BET area = 2322.0 m^2/g.

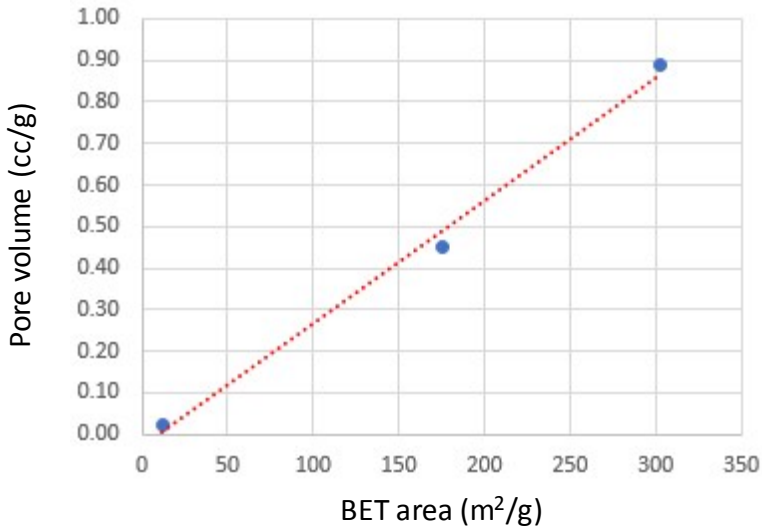

Figure S23. Correlation between BET area and pore volume for Ni-BM 65, Ni-BM-73 and Ni-BTC.

Table S1. List of linkers found in Ni MOFs encountered in the CoRE MOF Database [2]. The Cambridge Structural Database name of the corresponding MOF is listed at the top. Many entries include a 2D representation of the nodes the linkers are bound to within the MOFs, and how the linkers are bound to them. This list was obtained through our search for possible structures corresponding to the ones synthesized in this work. Images from Marvin Js [10] and Cambridge Structural Database [11]

ADOBUR	ADOCAY	ADOCIG
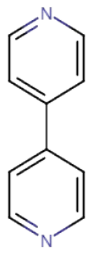	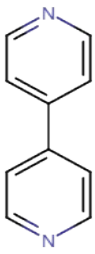	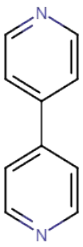

AFEDIA	AGUWUV	ALIXOJ
	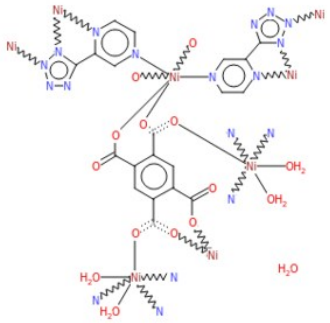	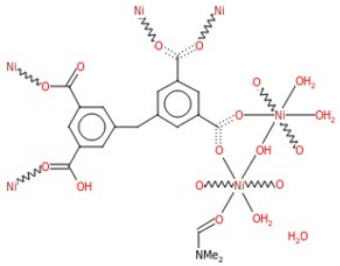
ALURIJ	AVELUJ	AVEMAQ
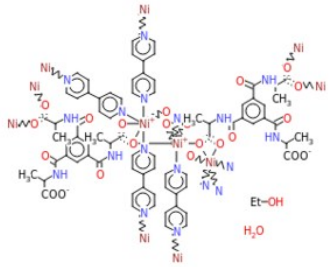	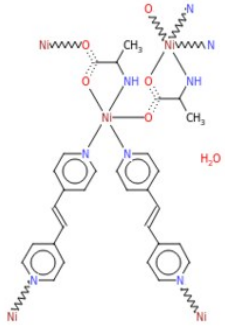	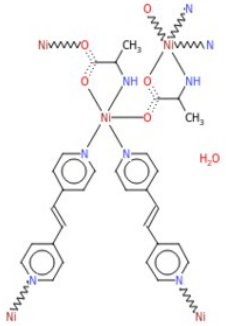
AXUBOL	BAKGIF	BEPROF
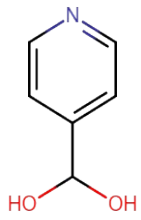	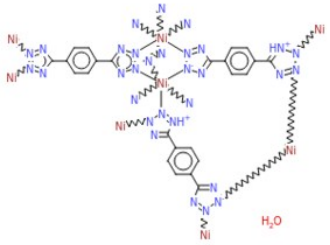	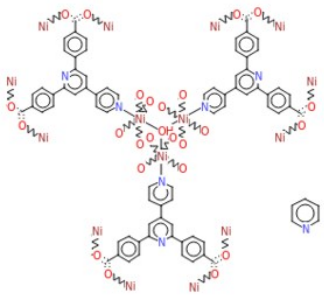

BEWRUR	BEWSAY	BEXPAX
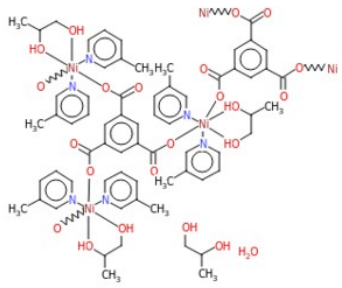	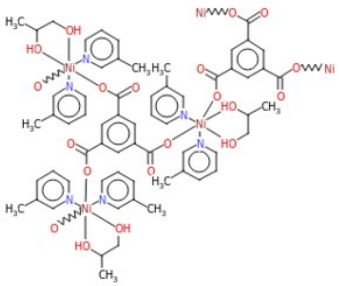	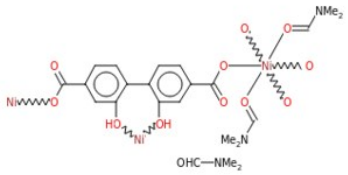
BEXRUT	BIBXOB	BIBXUH
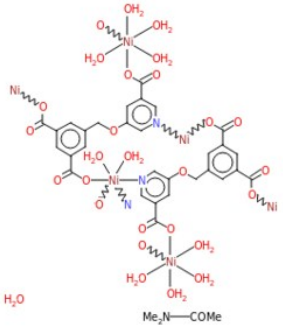	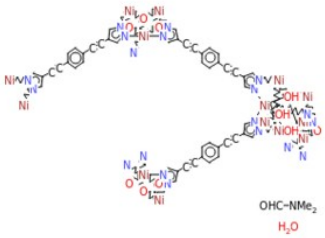	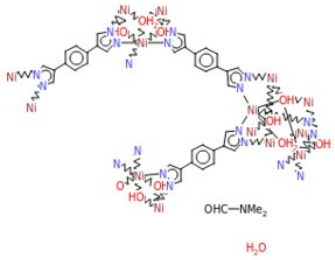
BINDAF	BONMEX	BORBEQ
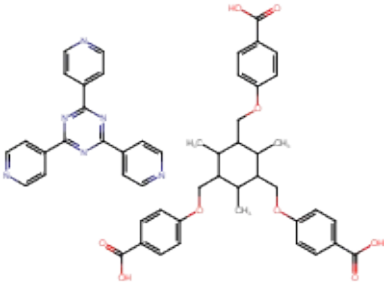	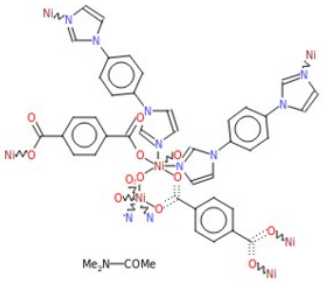	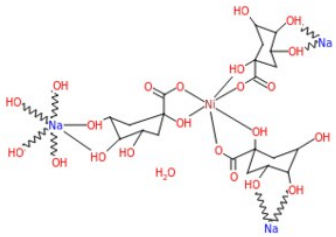

BUCROH	CAWZUX	CAXXEG
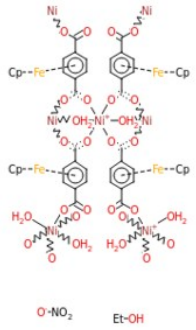	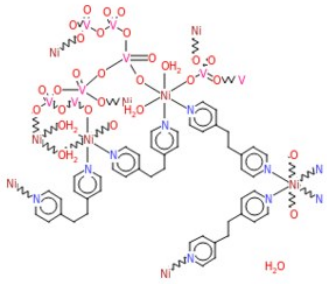	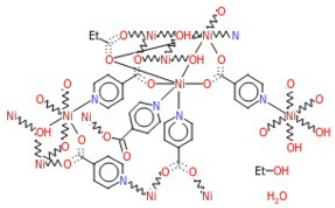
CEHWIX	CEHWOD	CETGOY
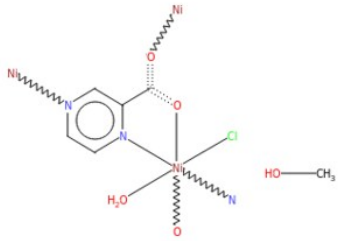	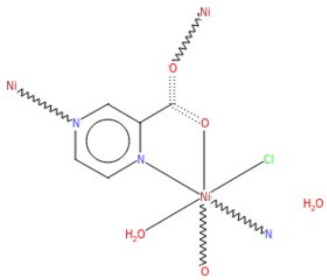	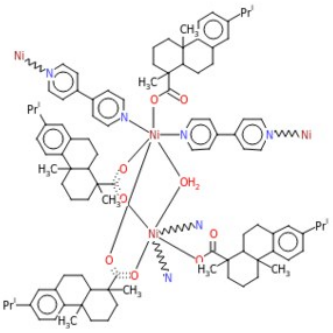
CIPRID	DAPXEZ	DAWBOU
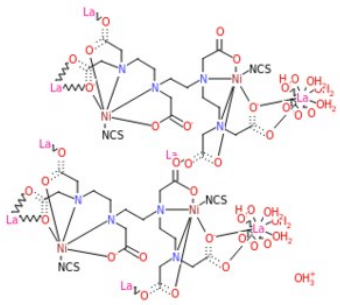		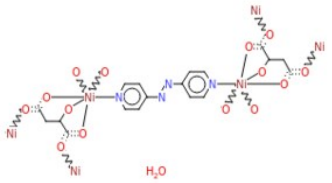

DAWCAH	DEYDOA	DEYJIC
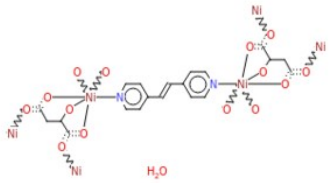	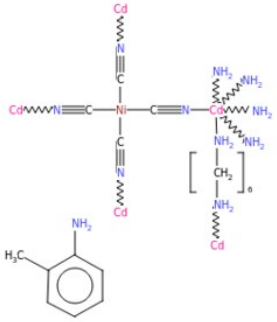	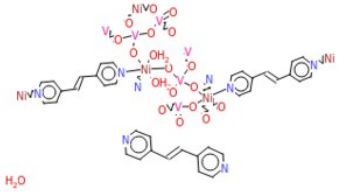
DIBPIP	DIBWUH	DODHUA
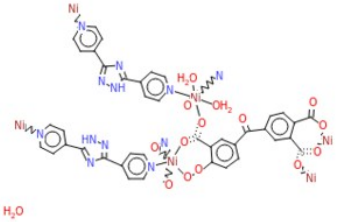	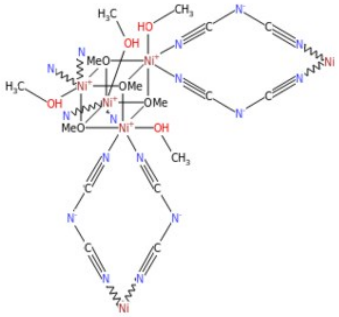	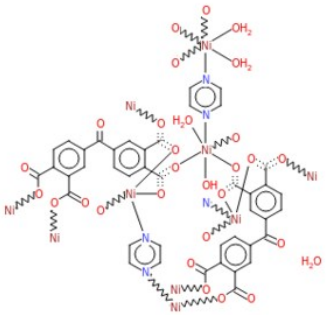
DOYLIM	DUXKEN	DUXZIG01
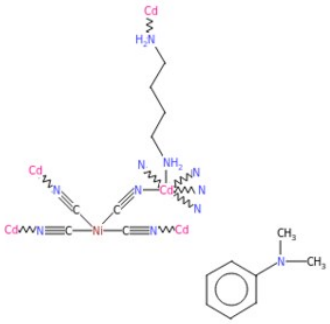	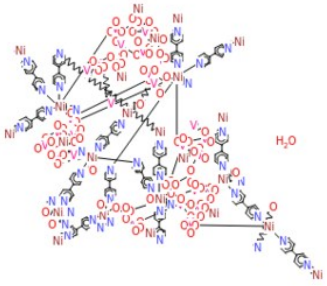	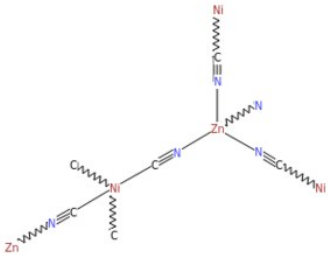

EBELUU	EBEMEF	ECEZAO
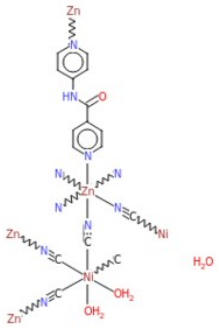	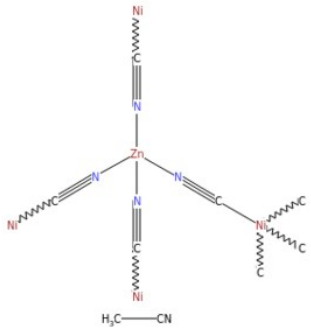	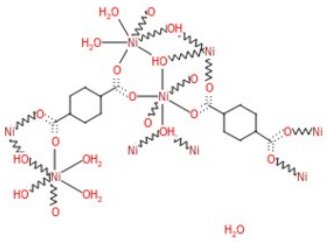
ECEZAO01	ECORIX	EGATIQ
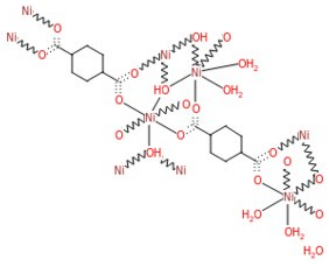	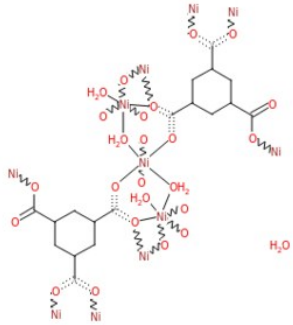	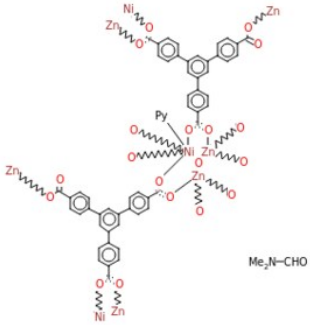
ENAFAB	ENUCOG	EXOTOB
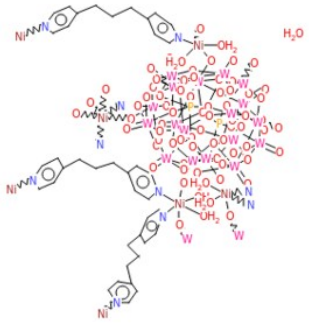	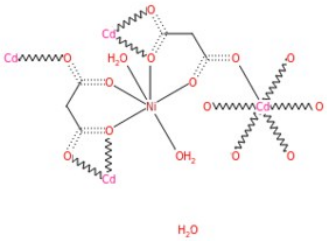	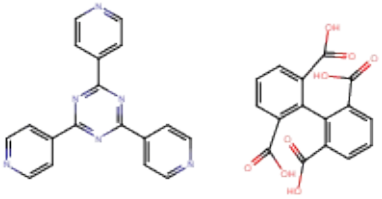

EZOFEF	FAKGOP	FEVDIV
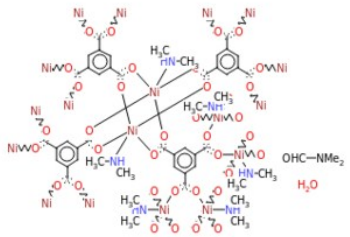	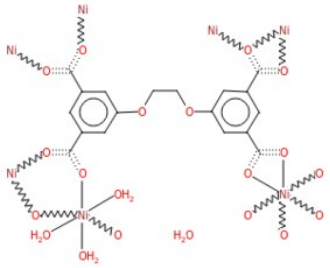	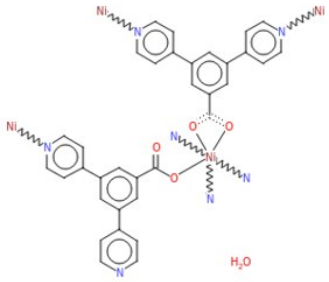
FEWTUY	FIFPAM	FIFPAM01
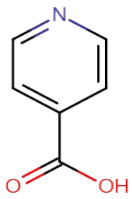	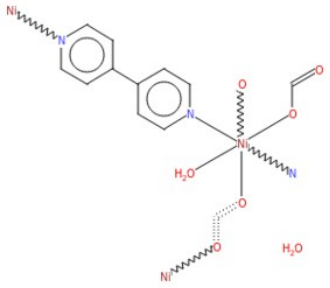	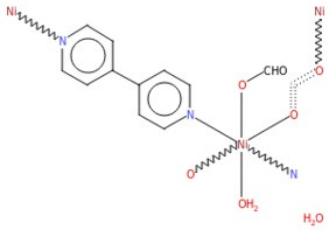
FIHRIZ	FISPIH	FOHSAW01
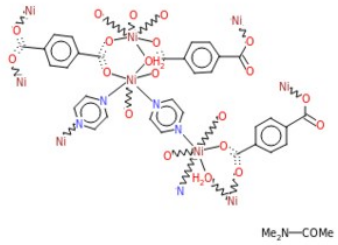	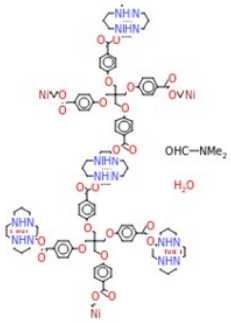	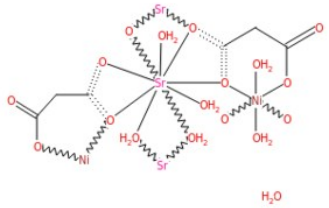

FUZKAN	GAGXAP	GAXQIH
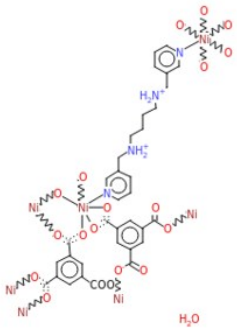	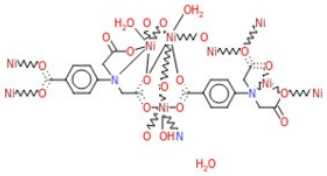	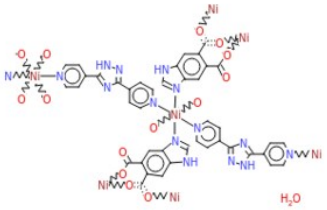
GEDDEA	GELVID	GELVID01
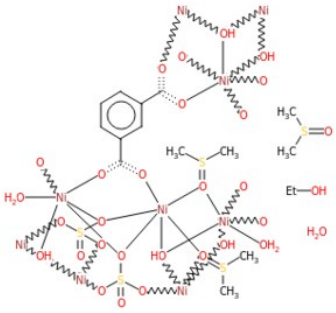	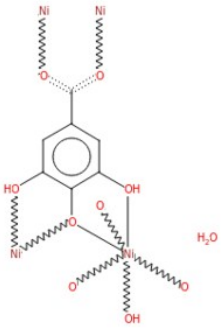	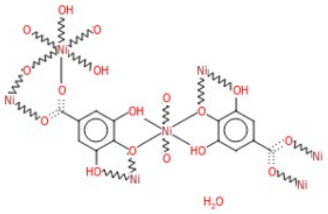
GESFAN	GIFKAH	GIFKIP
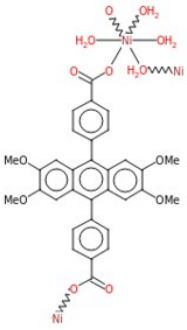	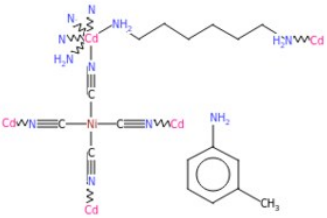	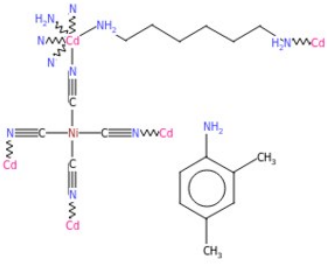

GIHPAQ	GUSCIH	HAFTOZ
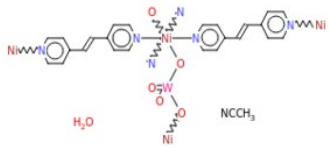	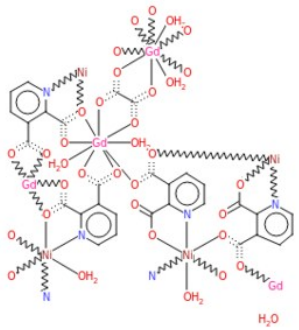	
HEDTER	HIFTUM	HIHFOV
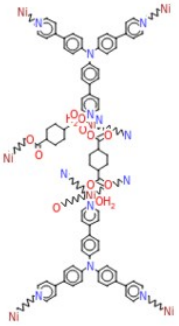	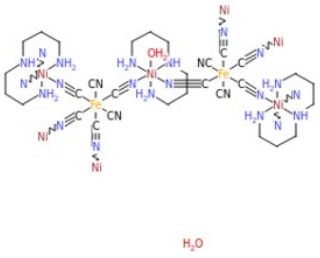	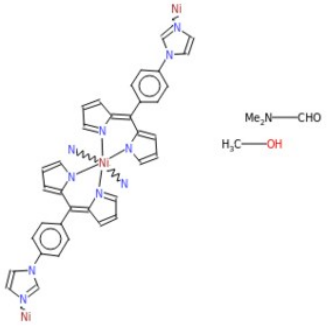
HIYYEU	HOGSIG	HURGUX
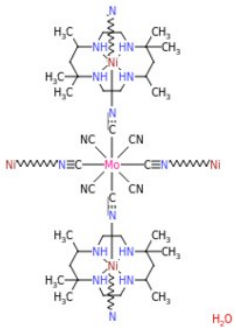	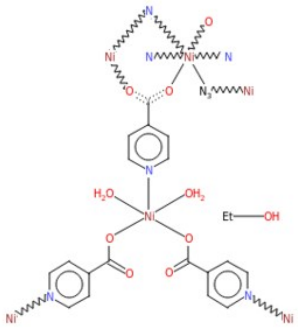	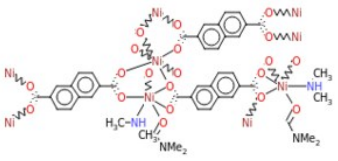

HURGUX01 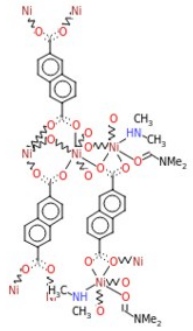	HUYJOA 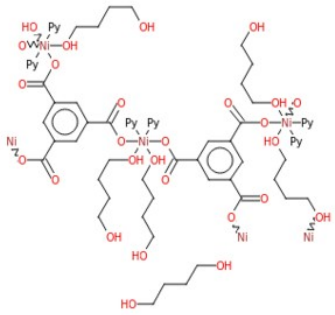	HUYJUG 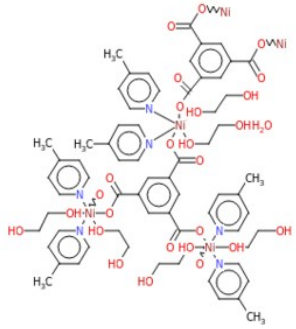
HUYKAN 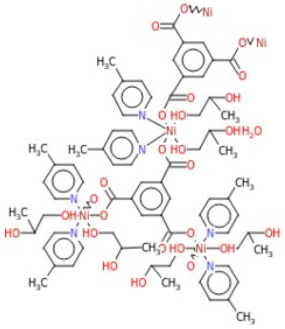	HUYKUH 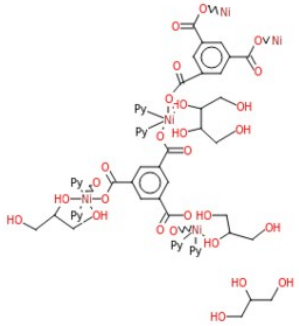	IBITUK 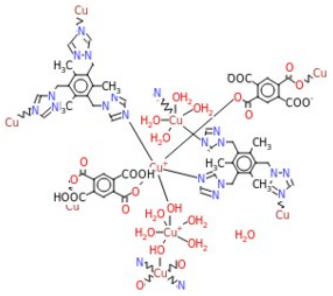
ICAROV 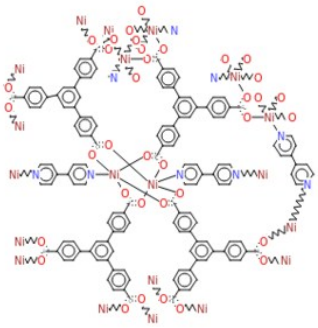	ICIVAS 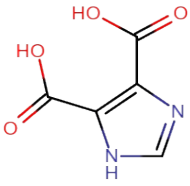	INEBOT 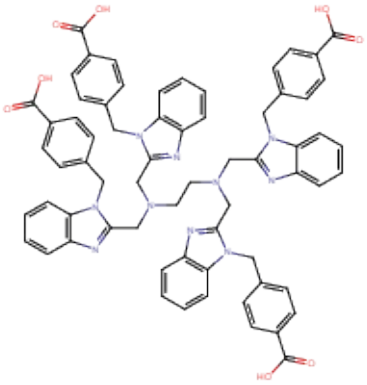

INEBOT01	INESIE	INIRAY
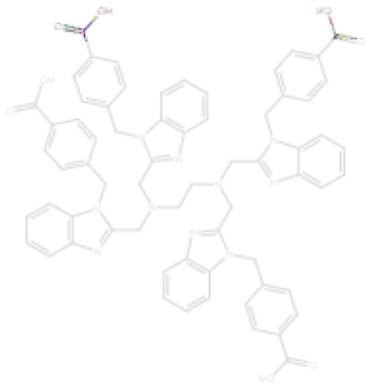	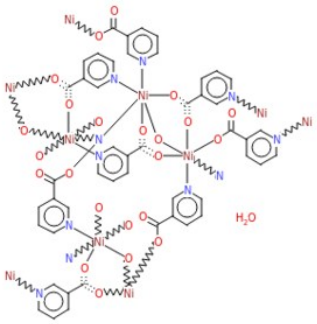	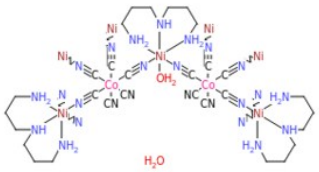
INIRAY01	ISENUQ	IYUREA
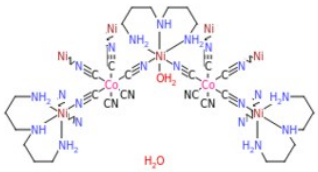	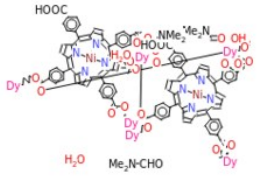	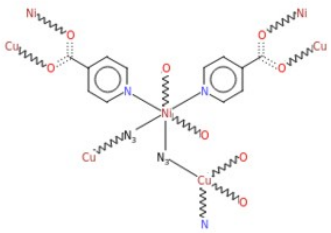
JEMNAR	KALFIO	KALFOU
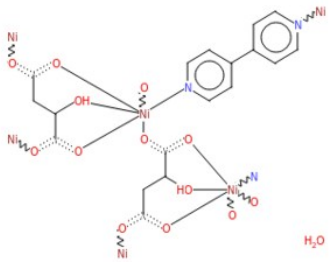	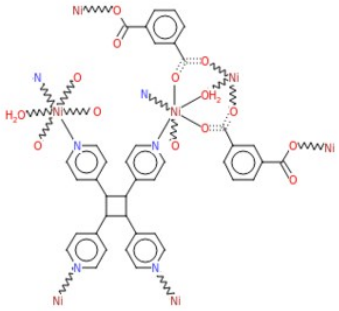	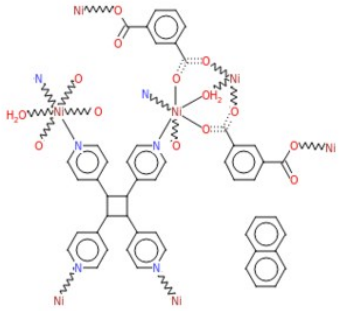

KALGAH	KALGEL	KARLIA
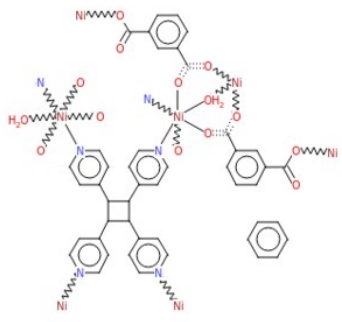	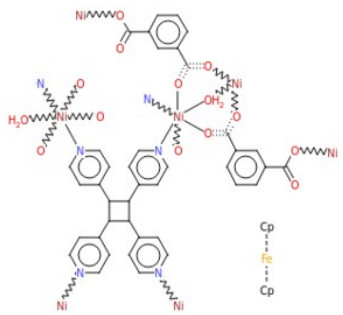	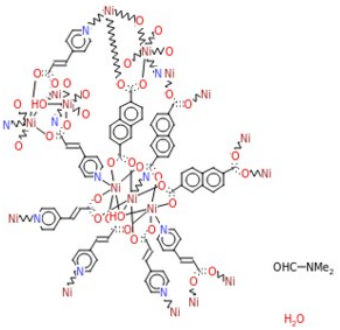
KARLUM	**KARMAT**	**KARNAU**
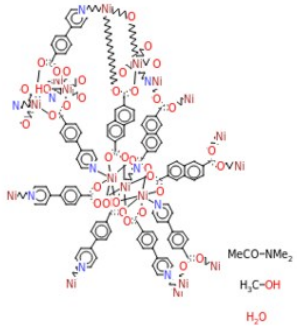	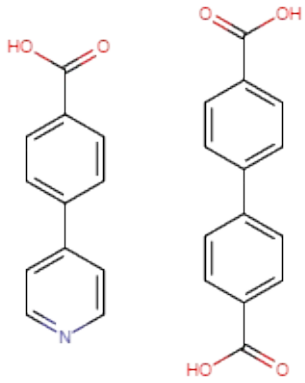	
KAVLID	**KEXFAU**	**KEYDEZ**
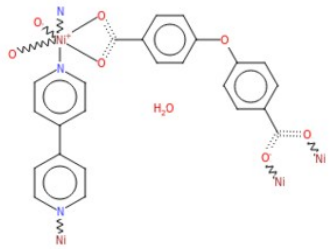	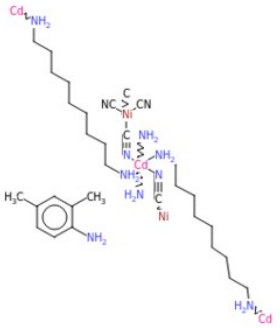	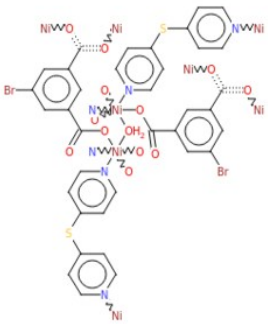

KIFXOO	KILFUI	KILFUI01
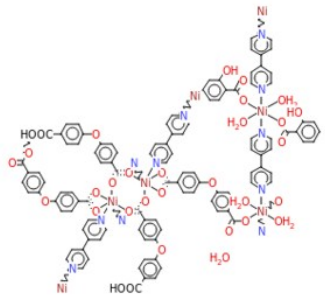	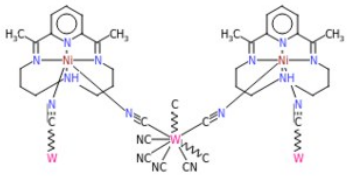	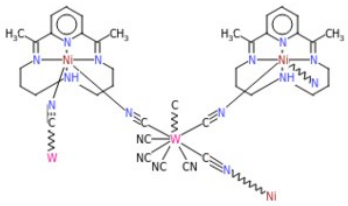
KINQAB	KIYMIP	KOLWEO
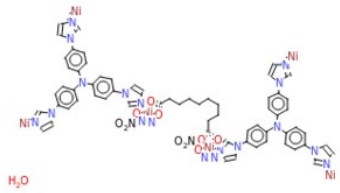	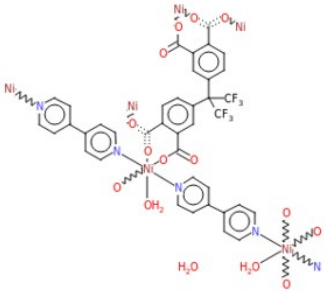	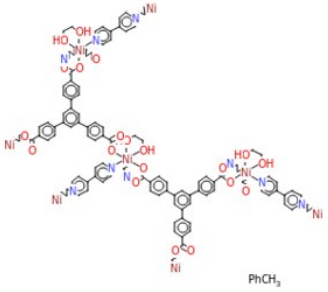
KONYOB	KUGZIW	KUJNEJ
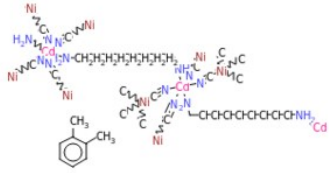	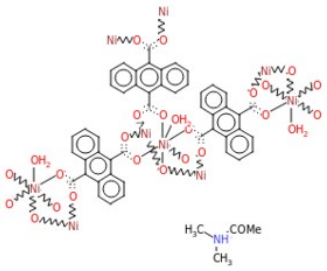	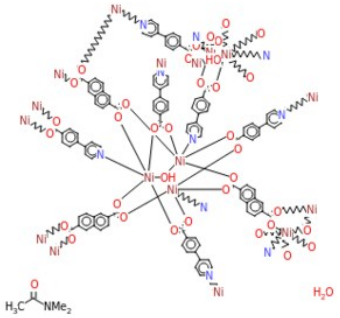

LASQON	LECQEQ	LEJRIC
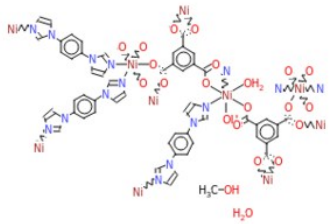	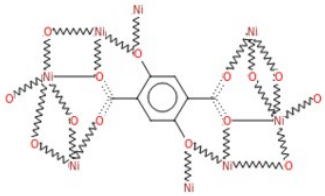	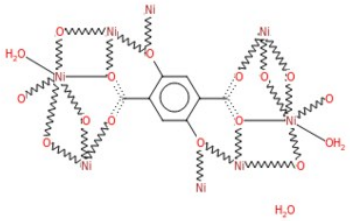
LOBHAM	LODPUQ	LOFCUF
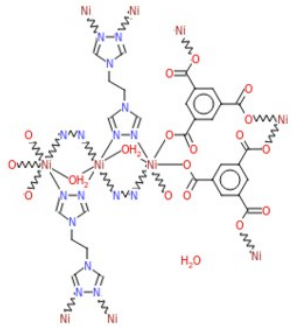	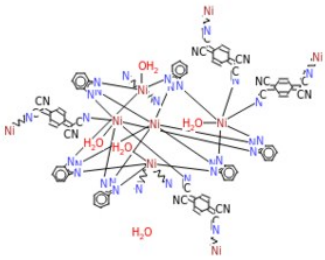	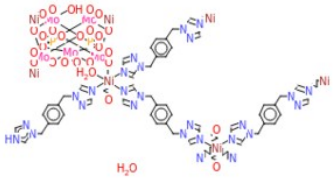
LOJNAA	LUFQUZ02	LULHUW
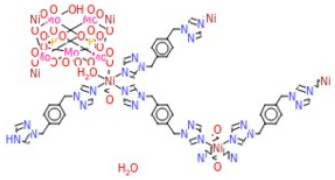	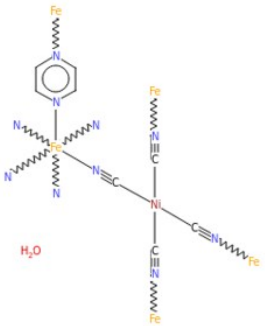	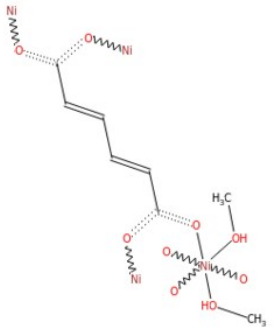

MARPOL	MEGBAD	MIFPUO
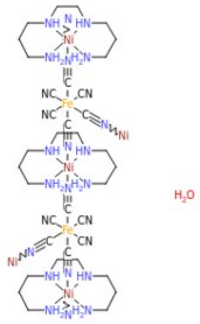		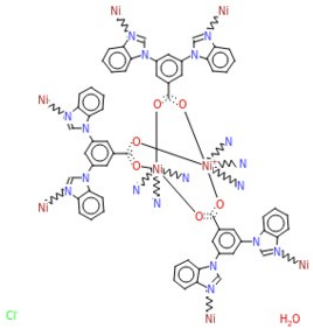
MIJMAU	MUGFOK	NEDWIE
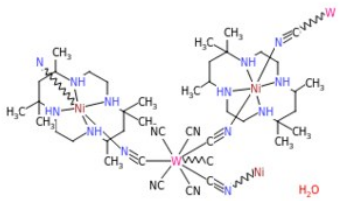	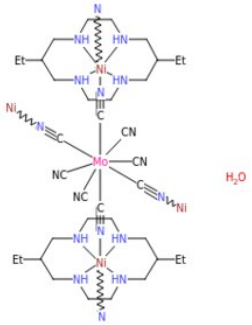	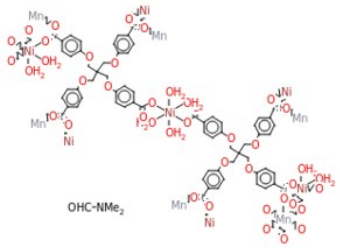
NERNON	NESTAI	NOKLIJ
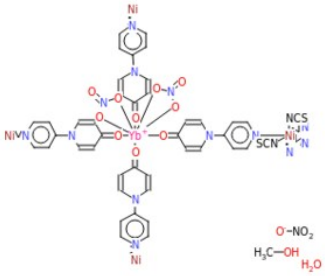	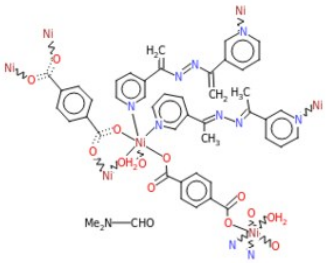	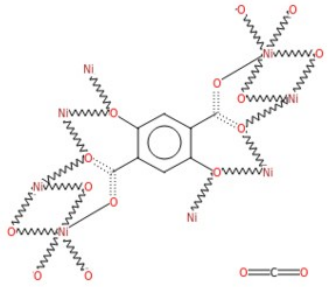

NUJCIE	NULMAJ	NUVYIN
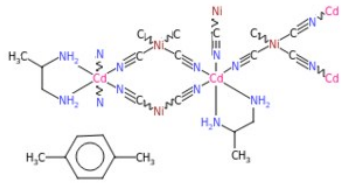	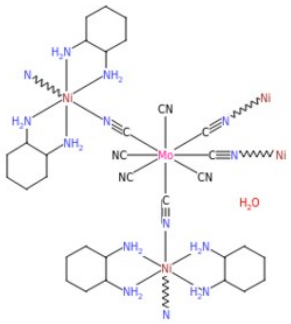	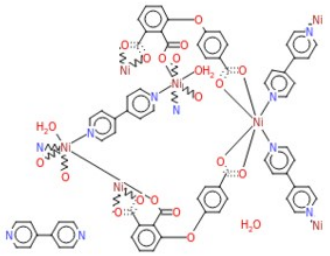
NUVYOT	OCAQOY	ODONEB
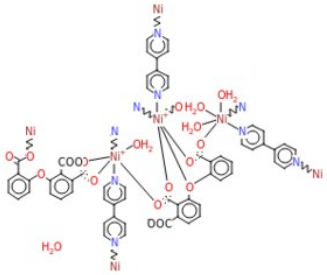	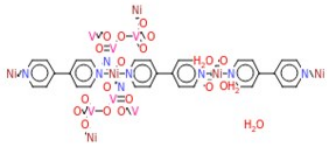	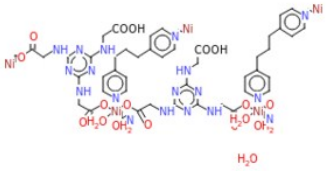
OGECOU	OLOKEF	OVIZID
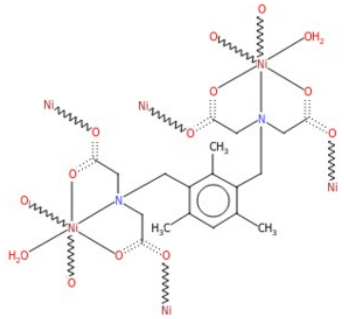	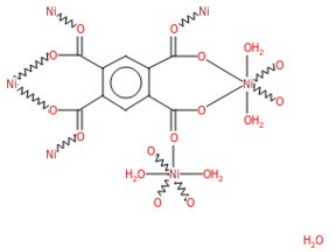	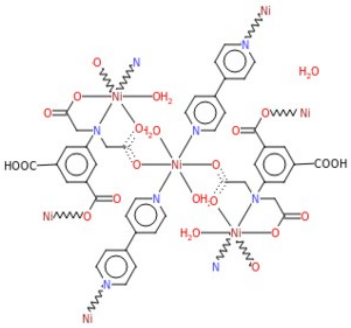

OYUJUO	PAPRUU	PAQVOU
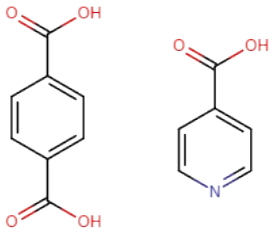	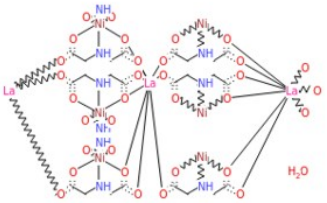	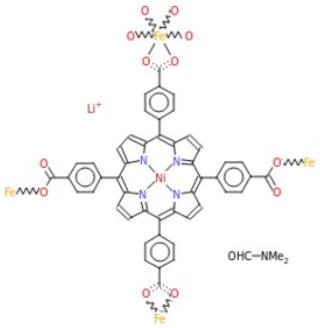
PARMIG	PEBXIF	PEPKUR
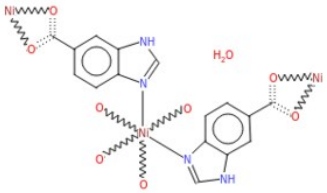	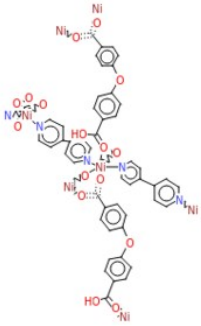	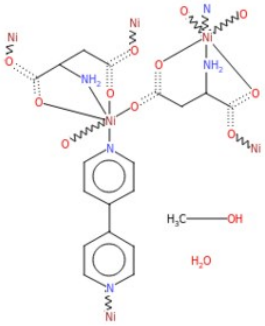
PESTUD	PEVXAQ	PEWXUL
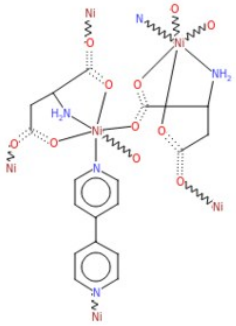	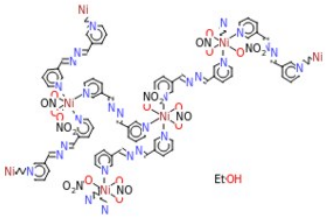	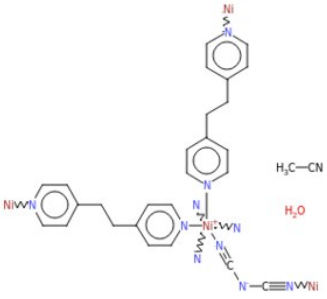

PEWXUL01	PEYSIW	POBYAH
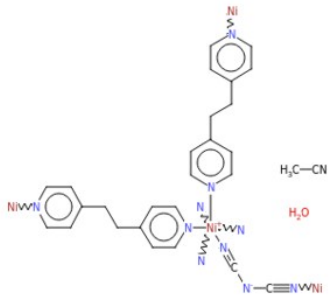	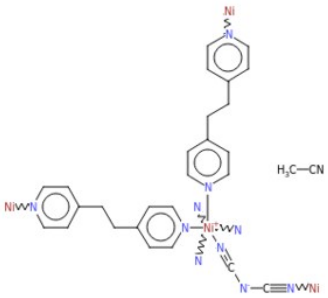	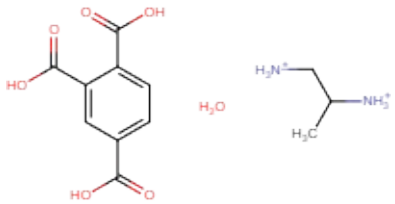
POKGEC	POQXAV	PUWCOZ
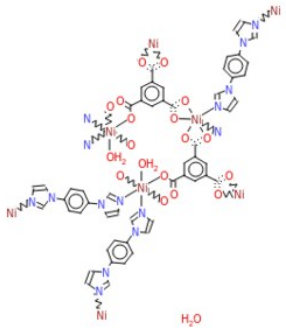	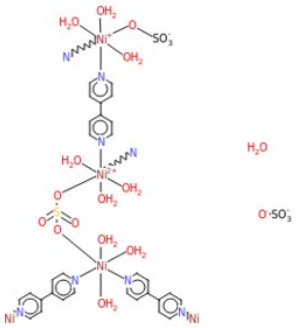	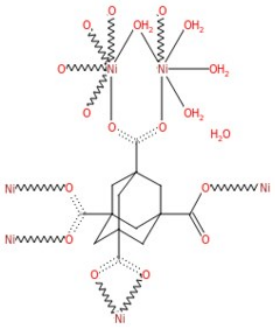
QAVYUJ	QAVZAQ	QERWAL
	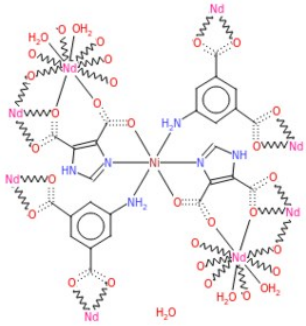	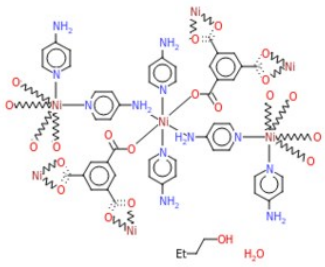

QOSXAY	QOVDEL	QUQGEP
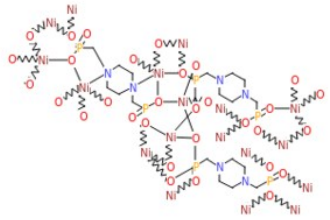	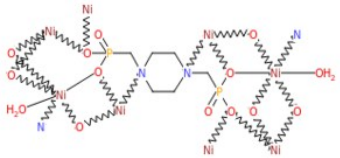	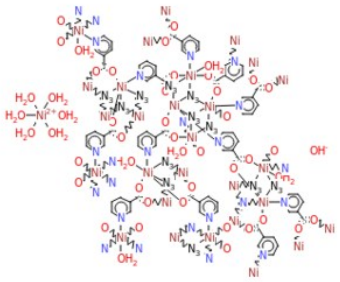
RABHAZ	RABHIH	RESSAK
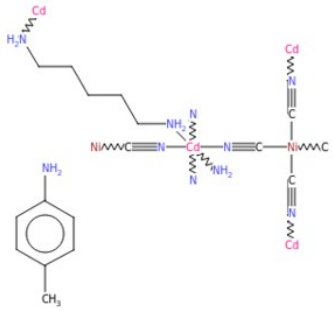	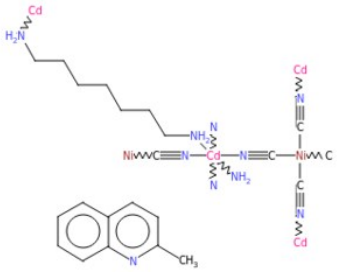	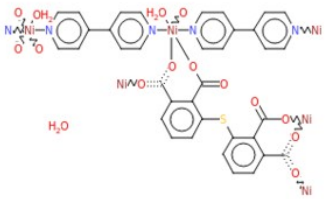
RIBDAJ	ROGLOP	ROGSAI
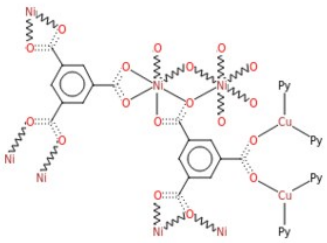	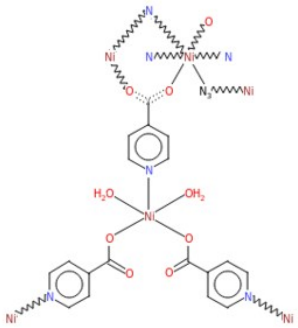	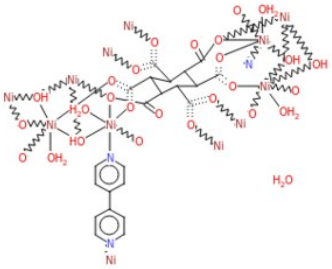

SEJBAL	SEQSIS	SISFEH
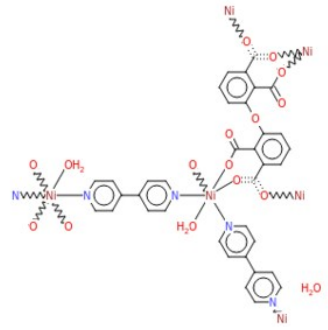	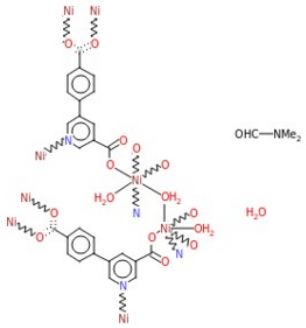	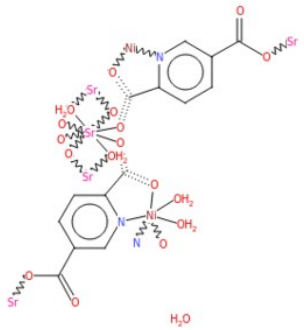
SIZPAT	SIZPEX	SOBZOY
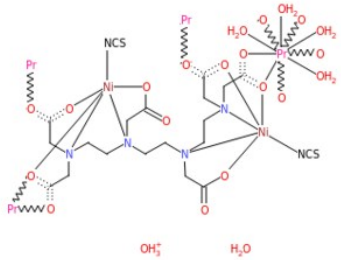	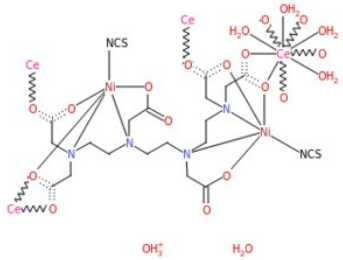	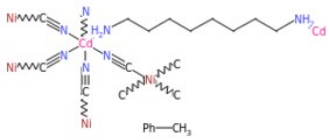
SOVHAM	TADYEE	TADYII
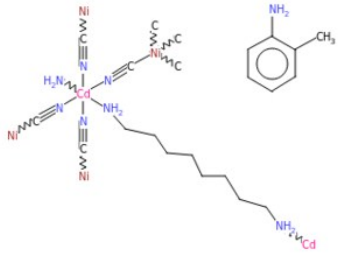	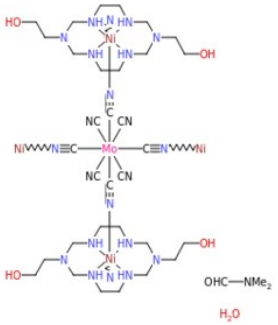	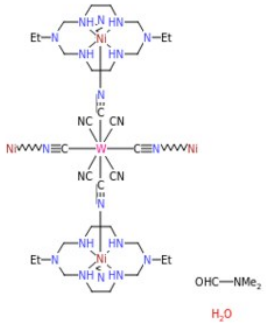

TARVUD	TISGUY	TOHPUC
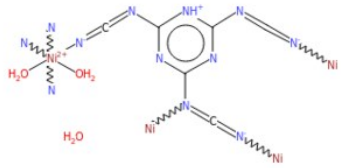	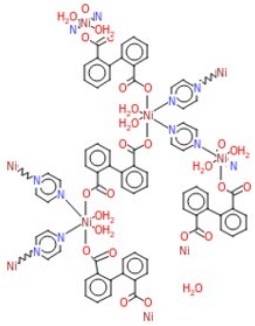	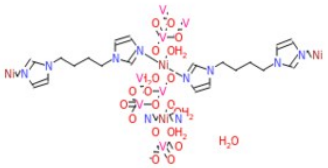
TONBUU	UDIHOF	UFATEA01
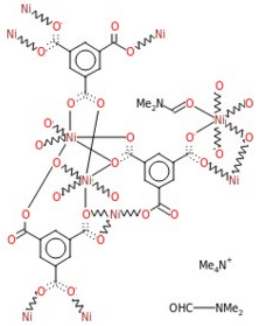	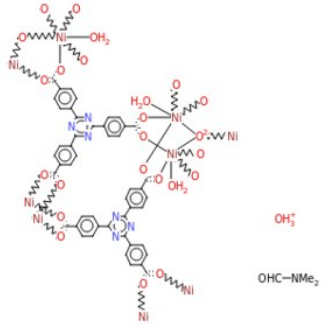	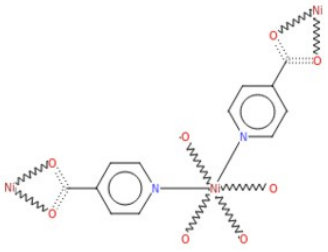
UGAQEY	UJARAZ	UQUHAQ
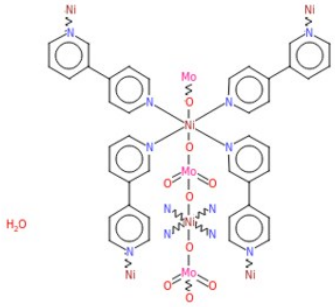	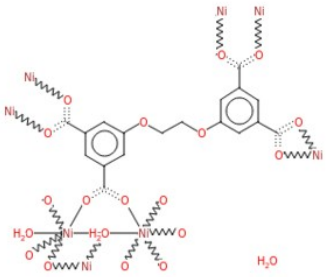	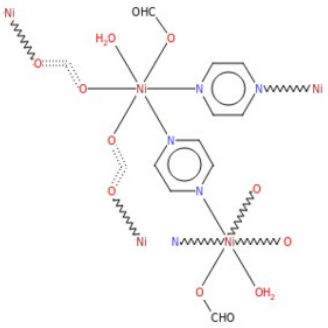

UTEWOG	UZAFAD	VECWUX
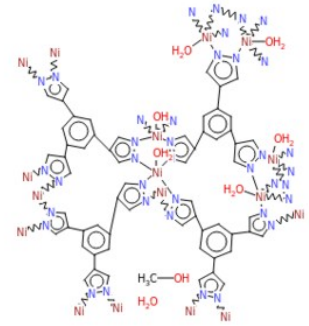	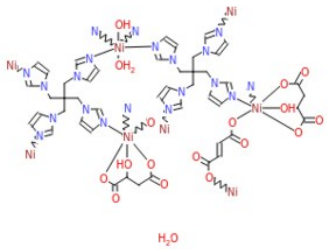	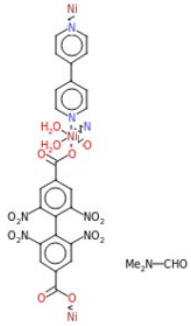
VEGXUC	VEHNED	VEQBID
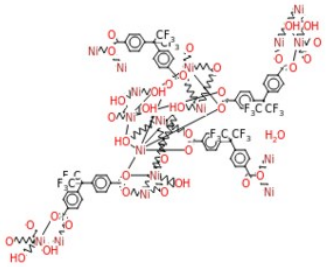	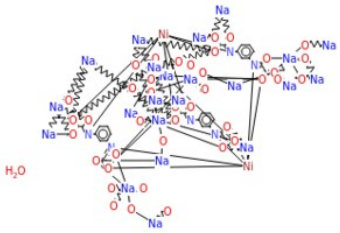	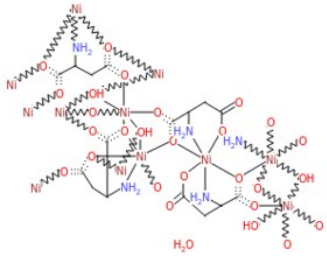
VETTAR	VEXTUO	VICLAW
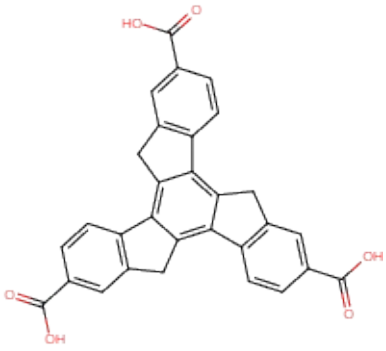		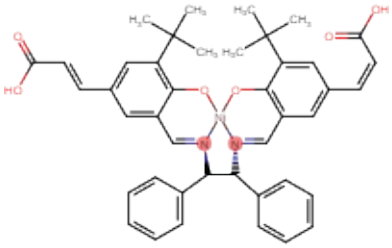

VIRPOC	VOCNOQ	VUSQIK
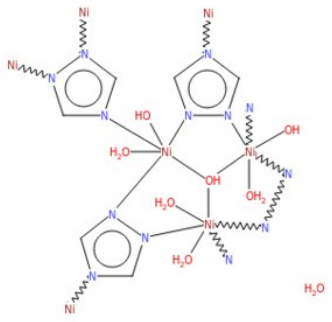	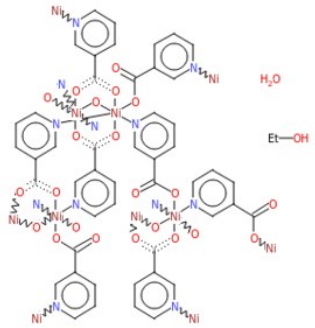	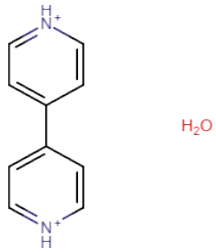
WARJAC	WEFXEM	WEFXIQ
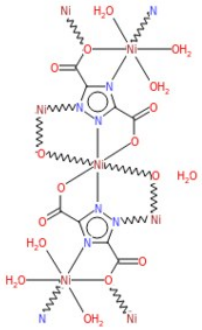	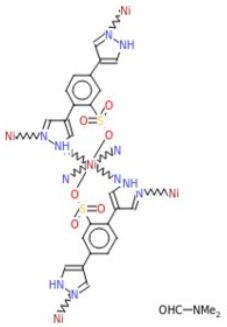	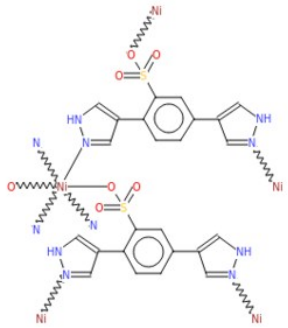
WEHPOP	WOWHEV	WUZRUE
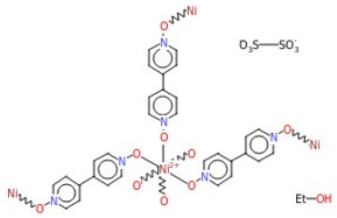	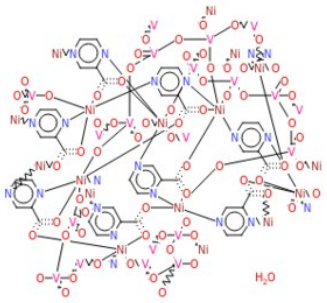	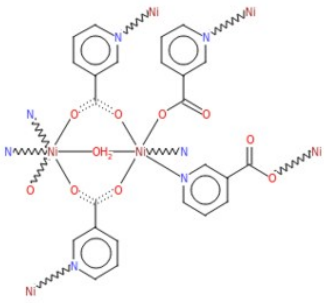

XADFEP	XAMLUS	XAPYAO
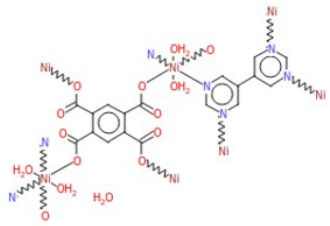	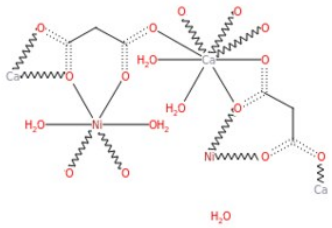	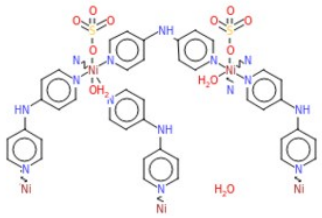
XEJXAN	XEJXER	XOBWIX
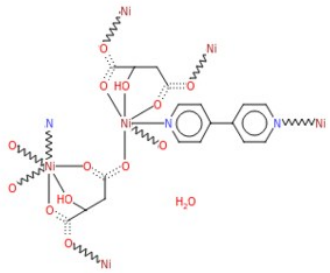	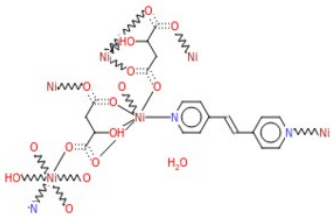	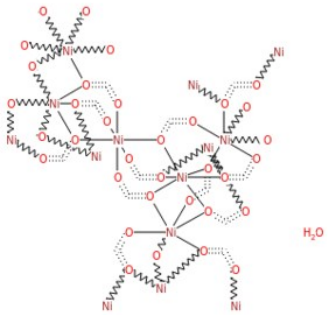
XOBXIW	XOJCUV	XOPVII
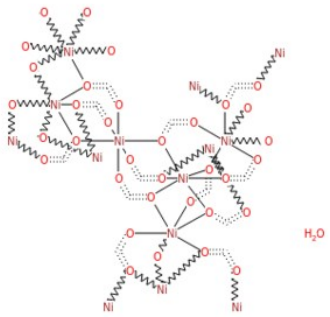	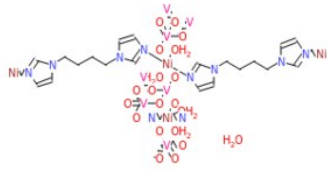	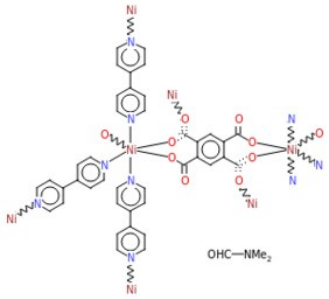

XUJCUB	XUTQEI	YAHPED
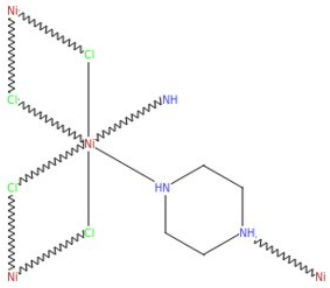	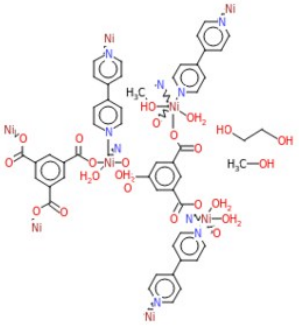	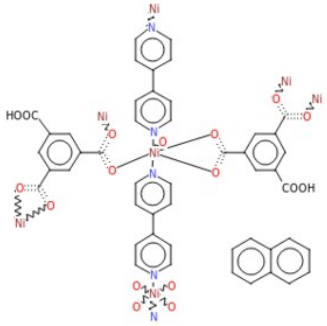
YAPMAF	YARBUQ	YEQRIV
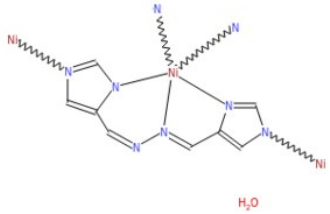	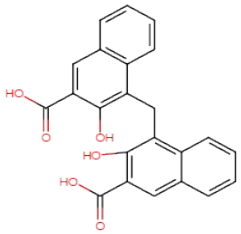	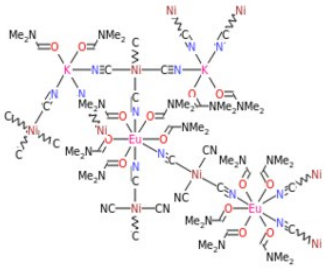
YERJEL	YEZKIZ	YIZWIN
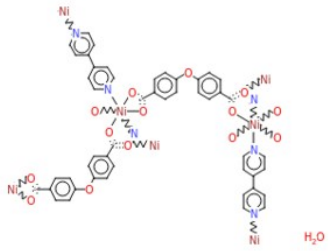	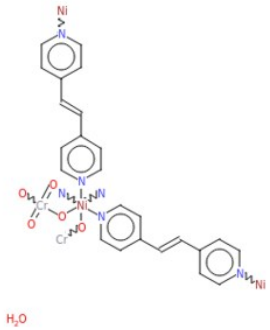	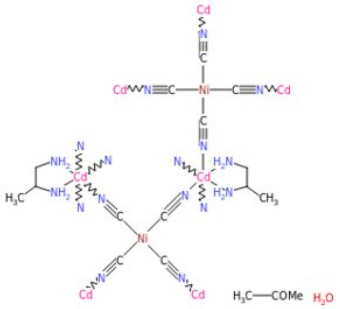

ZURQOS	ZURROT	
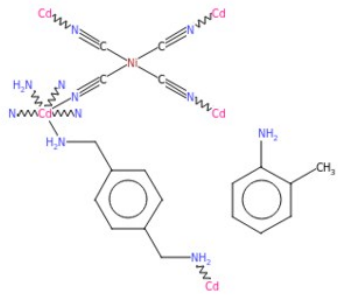	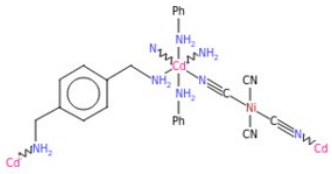	

REFERENCES

1. "Material Studio"; Accelrys Software Inc.: San Diego, CA 92121, USA, 2001- 2011.
2. Y. G. Chung, J. Camp, M. Haranczyk, B. J. Sikora, W. Bury, V. Krungleviciute, T. Yildirim, O. K. Farha, D. S. Sholl, and R. Q. Snurr, "Computation-ready, experimental metal-organic frameworks: A tool to enable high-throughput screening of nanoporous crystals," *Chem. Mater.*, vol. 26, no. 21, pp. 6185–6192, 2014.
3. Dubbeldam, D.; Calero, S.; Ellis, D. E.; Snurr, R. Q.RASPA: Molecular Simulation Software for Adsorption and Diffusion in Flexible Nanoporous Materials *Mol. Simul.* **2016**, 42, 81– 101
4. Rappe, A. K.; Casewit, C. J.; Colwell, K. S.; Goddard, W. A.; Skiff, W. M.Uff, a Full Periodic Table Force Field for Molecular Mechanics and Molecular Dynamics Simulations *J. Am. Chem. Soc.* **1992**, 114,10024–10035
5. Potoff, J. J.; Siepmann, J. I.Vapor–Liquid Equilibria of Mixtures Containing Alkanes, Carbon Dioxide, and Nitrogen *AIChE J.* **2001**, 47, 1676– 1682
6. Gelb, L. D.; Gubbins, K. E.Pore Size Distributions in Porous Glasses: A Computer Simulation Study*Langmuir* **1999**, 15, 305– 308
7. Gomez-Gualdron, D. A.; Colon, Y. J.; Zhang, X.; Wang, T. C.; Chen, Y.-S.; Hupp, J. T.; Yildirim, T.;Farha, O. K.; Zhang, J.; Snurr, R. Q.Evaluating Topologically Diverse Metal-Organic Frameworks for Cryo-Adsorbed Hydrogen Storage *Energy Environ. Sci.* **2016**, 9, 3279– 3289
8. M.J. Frisch, G.W. Trucks, H.B. Schlegel, G.E. Scuseria, M.A. Robb, J.R. Cheeseman, G. Scalmani, V. Barone, B. Mennucci, G.A. Petersson, H. Nakatsuji, M. Caricato, X. Li, H.P. Hratchian, A.F. Izmaylov, J. Bloino, G. Zheng, J.L. Sonnenberg, M. Hada, M. Ehara, K. Toyota, R. Fukuda, J. Hasegawa, M. Ishida, T. Nakajima, Y. Honda, O. Kitao, H. Nakai, T. Vreven, J.A. Montgomery Jr., J.E. Peralta, Fo Ogliaro, M.J. Bearpark, J. Heyd, E.N. Brothers, K.N. Kudin, V.N. Staroverov, R. Kobayashi, J. Normand, K. Raghavachari, A.P. Rendell, J.C. Burant, S.S. Iyengar, J. Tomasi, M. Cossi, N. Rega, N.J. Millam, M. Klene, J.E. Knox, J.B. Cross, V. Bakken, C. Adamo, J. Jaramillo, R. Gomperts, R.E. Stratmann, O. Yazyev, A.J. Austin, R. Cammi, C. Pomelli, J.W. Ochterski, R.L. Martin, K. Morokuma, V.G. Zakrzewski, G.A. Voth, P. Salvador, J.J. Dannenberg, S. Dapprich, A.D. Daniels, O. Farkas, J.B. Foresman, J.V. Ortiz, J. Cioslowski, D.J. Fox **Gaussian 09**, Gaussian, Inc., Wallingford, CT, USA (2009)
9. Y. Zhao & D.G. Truhlar (2006). "The M06 suite of density functionals for main group thermochemistry, thermochemical kinetics, noncovalent interactions, excited states, and transition elements: Two new functionals and systematic testing of four M06-class functionals and 12 other functionals". *Theor Chem Account*. **120**: 215–241
10. Marvin was used for drawing and displaying chemical structures, Marvin 17.2.6, 2017 , ChemAxon (http://www.chemaxon.com)
11. C. R. Groom, I. J. Bruno, M. P. Lightfoot, and S. C. Ward, "The Cambridge structural database," *Acta Crystallogr. Sect. B Struct. Sci. Cryst. Eng. Mater.*, vol. 72, no. 2, pp. 171–179, 2016